Probiotics and Antimicrobial Proteins
https://doi.org/10.1007/s12602-026-11247-9

RESEARCH

# A Novel Cationic Antimicrobial Peptide Scymidgutin$_{8–29}$ from *Scylla paramamosain* with Antimicrobial and Anti-inflammatory Activities and Therapeutic Potential in DSS-induced Colitis in Mice

**Chang Zhang[1] · Xianxian Dong[1] · Ning Ding[1] · Fangyi Chen[1,2,3] · Ke-Jian Wang[1,2,3]**

Received: 20 May 2026 / Accepted: 5 October 2026
© The Author(s), under exclusive licence to Springer Science+Business Media, LLC, part of Springer Nature 2026

## Abstract

Marine-derived antimicrobial peptides possess both antibacterial and immunomodulatory activities, offering potential advantages for treating complex inflammatory conditions. Meanwhile, the management of inflammatory bowel disease is complicated by the interplay of microbial dysbiosis and bacterial-driven inflammation, which conventional single-target therapies frequently fail to address. In this study, we identified a novel cationic antimicrobial peptide, Scymidgutin$_{8–29}$, from the mud crab *Scylla paramamosain*. This 22-residue peptide possesses a calculated molecular mass of 2658.23 Da, an estimated pI of 12.31, and 37.5% hydrophobicity. Scymidgutin$_{8–29}$ exhibited potent, broad-spectrum membrane-disrupting activity against clinically relevant pathogens, including multidrug-resistant strains, with MBCs of 1.5-3 μM against the tested multidrug-resistant *Acinetobacter baumannii* isolates and 6–12 μM against MRSA isolates, achieving > 99.9% killing within 20 min. Furthermore, the peptide demonstrated potent anti-inflammatory activity by promoting M2 macrophage polarization in LPS-stimulated RAW264.7 cells, as evidenced by the downregulation of iNOS (to 0.24-fold of LPS control), NO (to 0.47-fold), and pro-inflammatory cytokines (IL-1β, TNF-α, IL-6 to 0.67-0.73-fold), along with the upregulation of Arg-1 (to 1.80-fold) and IL-10 (to 1.38-fold). In a dextran sulfate sodium (DSS)-induced acute colitis mouse model, intrarectal administration of Scymidgutin$_{8–29}$ (5 mg/kg) significantly reduced the disease activity index (from 7.0 to 3.0), restored colonic histopathology, rebalanced cytokine profiles, and altered gut microbiota composition, notably decreasing colitis-associated *Akkermansia* and *Proteobacteria*. These results indicate that Scymidgutin$_{8–29}$ possesses both direct membrane-disruptive antibacterial activity and immunomodulatory capacity, and demonstrates therapeutic efficacy in the DSS-induced colitis model, positioning it as a potential multi-functional therapeutic candidate for intestinal inflammation.

**Keywords** Scymidgutin$_{8–29}$ · Marine antimicrobial peptide · Membrane disruption · Macrophage polarization · DSS-induced colitis

✉ Fangyi Chen
chenfangyi@xmu.edu.cn

✉ Ke-Jian Wang
wkjian@xmu.edu.cn

[1] State Key Laboratory of Marine Environmental Science, College of Ocean & Earth Sciences, Xiamen University, Xiamen, Fujian 361102, China

[2] State-Province Joint Engineering Laboratory of Marine Bioproducts and Technology, College of Ocean & Earth Sciences, Xiamen University, Xiamen, Fujian, China

[3] Marine Biological Antimicrobial Peptide Industry Research Institute, Fujian Ocean Innovation Center, Xiamen, Fujian, China

## Introduction

Inflammatory bowel disease (IBD), encompassing Crohn's disease and ulcerative colitis, is a chronic relapsing disorder characterized by intestinal inflammation, epithelial barrier dysfunction, and gut microbiota dysbiosis; its global incidence is increasing [1–3]. The pathogenesis of IBD involves a complex interplay in which impaired barrier integrity and diminished host defense peptide secretion coincide with a reduction in microbial α-diversity and an expansion of pro-inflammatory bacteria, such as adherent-invasive *Escherichia coli*, along with a decline in protective species, such as *Faecalibacterium prausnitzii* [4–11].

Published online: 10 October 2026

Current mainstay therapies, including immunosuppressants and biologics, often fail to provide sustained remission, increase infection risks, and critically do not directly correct the underlying microbial dysbiosis [12–15]. This gap underscores the imperative to develop novel strategies that can concurrently target pathogenic bacteria and recalibrate the dysregulated host immune response [16]. In this context, bioactive natural compounds with both antimicrobial and immunomodulatory activities are of considerable interest.

Antimicrobial peptides (AMPs), which are key effector molecules of innate immunity, represent a promising class of such agents. Beyond their direct microbicidal activity via membrane disruption, many AMPs possess immunomodulatory functions, including the inhibition of pro-inflammatory pathways and modulation of macrophage polarization [17–20]. In the intestinal tract, Paneth cell-derived defensins exemplify this dual functionality: these peptides not only maintain crypt sterility and shape the local microbiome, but also participate in the regulation of mucosal immune responses and epithelial barrier function [21–23]. Reduced expression of Paneth cell α-defensins in ileal Crohn's disease and inadequate induction of β-defensins in colonic IBD highlight the pathogenic significant of AMP deficiency in intestinal inflammation [21, 22]. Notably, exogenous administration of certain defensins has been shown to mitigate experimental colitis through immunomodulatory mechanisms independent of their direct antimicrobial activity [23].

Peptides have been increasingly recognized as a promising class of therapeutics for inflammatory and regenerative disorders. Recent peptide-based interventions have demonstrated significant potency in modulating inflammation and preserving barrier integrity. Notably, amphibian-derived peptides such as OA-AL14 and OL-RA11, exhibit diverse bioactivities, including anti-photoaging, anti-vascular aging, and wound healing properties [24–26]. These effects are often mediated by immunomodulatory mechanisms such as autophagy regulation and macrophage polarization [27, 28]. Similar multifunctional properties have been reported for food-derived peptides in mucosal repair [29]. Together, these findings reinforce the concept that AMPs can serve as dual-functional agents, simultaneously targeting microbial pathogens and modulating host immune responses.

Marine organisms, particularly crustaceans thriving in pathogen-rich environments, have evolved a diverse repertoire of AMPs as primary defense mechanisms, representing an underexplored reservoir for therapeutic discovery [30, 31].Although crustacean AMPs, such as anti-lipopolysaccharide factors (ALFs) and crustins, are known for their broad-spectrum antimicrobial activities in vitro, their potential to ameliorate mammalian intestinal inflammation through combined antimicrobial and immunomodulatory actions remains largely unexplored [32, 33].

We identified a novel gene, *Scymidgutin* (GenBank accession OP218848), from the transcriptome of pathogen-challenged mud crab (*Scylla paramamosain*) in our laboratory. Through bioinformatic analysis of its physicochemical properties and structural features, a 22-amino acid cationic core peptide, Scymidgutin$_{8–29}$, was rationally designed.

In the present study, we sought to comprehensively characterize the antimicrobial mechanism of Scymidgutin$_{8–29}$ and evaluate its therapeutic potential in intestinal inflammation. Specifically, we investigated its in vitro antimicrobial spectrum, killing kinetics, stability, and membrane-disruptive mechanism against clinically relevant pathogens, including multidrug-resistant strains. Its immunomodulatory capacity was assessed by examining macrophage polarization in LPS-stimulated RAW264.7 cells and neutrophil trafficking in zebrafish larvae. Furthermore, in a dextran sulfate sodium (DSS)-induced acute colitis mouse model, we evaluated its ability to alleviate colitis symptoms, modulate cytokine profiles, and alter gut microbiota composition. Our findings indicate that Scymidgutin$_{8–29}$ combines direct membrane-disruptive antibacterial activity with immunomodulatory properties and shows therapeutic efficacy in experimental colitis, positioning it as a multi-functional candidate worthy of further investigation.

## Materials and Methods

### Animal and Cell Resources

Adult mud crabs (300 ± 10 g) were obtained from an aquaculture facility in Zhangpu County, Fujian Province, China, and acclimatized for at least 72h before dissection. Multiple tissues (hemocytes, muscle, gills, epidermis, hepatopancreas, midgut, brain, gonads, and associated reproductive tissues) were collected from healthy males and females. Developmental stages, including embryos (I-V), zoea larvae (I-V), megalopa, and juveniles were collected systematically.

Transgenic zebrafish (*Danio rerio*; Tg (lyz: DsRed)) were kindly provided by Prof. Li Mingyu (Xiamen University) and maintained in flow-through systems at 28.0 ± 0.5 °C under a twice-daily artemia feeding regimen. All experimental procedures utilized MS-222 anesthesia (0.4%; Sigma-Aldrich, USA). Female C57BL/6 mice (6–8 weeks old; GemPharmatech Co., Ltd., Nanjing) were housed in individually ventilated cages (IVCs; 5 mice/cage) under standardized conditions (21 ± 1 °C, 40–70% relative humidity, 12 h light/dark cycle), with ad libitum access to food and water. All animal procedures were approved by the

Institutional Animal Care and Use Committee (IACUC) of Xiamen University (Approval No. XMULAC20240082).

HEK293T and RAW264.7 cell lines were obtained from the National Collection of Authenticated Cell Cultures (Shanghai, China) and cultured in DMEM (Gibco, USA) supplemented with 10% fetal bovine serum (FBS; Gibco, USA) at 37 °C under 5% $CO_2$. ZF4 cells, a zebrafish embryonic fibroblast line (China Zebrafish Resource Center, Wuhan), were cultured in DMEM/F12 (1:1; Gibco, USA) supplemented with 10% FBS at 28 °C under 5% $CO_2$.

## Transcriptome Mining and cDNA Cloning

A previously uncharacterized gene exhibiting significant upregulation following V. alginolyticus challenge was identified using our established mud crab transcriptome database. Gene-specific primers (Supplementary Table 1) were designed from predicted sequences to amplify the full-length cDNA, using cDNA pools from multiple tissues as templates. Protein physicochemical parameters were calculated computationally using the ExPASy Proteomics Server (https://www.expasy.org/).

Total RNA was isolated from tissue samples using TRIzol™ Reagent (Thermo Fisher Scientific, USA), and concentrations were determined using NanoDrop™ 2000 spectrophotometry (Thermo Fisher Scientific, USA). After cDNA synthesis, primer specificity was confirmed by melt curve analysis. qPCR was conducted on an ABI 7500 Real-Time PCR System (Applied Biosystems, USA) with FastStart™ SYBR Green Master Mix (Roche, Germany) under the following conditions: initial denaturation at 95 °C for 10 min; 40 cycles of 95 °C for 15 s and 60 °C for 1 min. Absolute quantification of Scymidgutin expression in various developmental stages and tissues utilized a standardized cDNA dilution series, with transcript levels normalized to endogenous β-actin and GAPDH references.

## Antimicrobial Peptide Design and Recombinant Expression Preparation

The bioactive domains of Scymidgutin were predicted through computational analysis of its amino acid sequence using the CAMPR3 antimicrobial peptide database. Employing physicochemical propensity scoring, we rationally designed a 22-residue truncated peptide ($Scymidgutin_{8–29}$: LPWTRLHSKKRGVLLRLQLSQK) corresponding to residues 8–29 of the mature protein. The sequence of $Scymidgutin_{8–29}$ and its related application have been disclosed in a Chinese patent application [34].

The *Escherichia coli* DH5α and BL21(DE3) strains harboring the pET-21a vector were cultured in lysogeny broth (LB). The codon-optimized $Scymidgutin_{8–29}$ gene (Sangon Biotech, China) was inserted into pET-21a-Mxe-ELK16 using NdeI/XhoI restriction sites. The construct's authenticity was confirmed by sequencing (Sangon Biotech, China).

The recombinant BL21(DE3) transformants were grown in LB medium supplemented with ampicillin (50 mg/L) at 37 °C until an $OD_{600}$ of 0.6–0.8 was reached. Protein expression was induced by adding 0.1 mM isopropyl β-D-1-thiogalactopyranoside (IPTG) and incubating at 16 °C for 24 h. Cells were pelleted by centrifugation (8,000 × *g*, 20 min, 4 °C) and lysed in buffer B1 (20 mM Tris-HCl, 500 mM NaCl, 1 mM EDTA, pH 8.5) via high-pressure homogenization at 800 bar. Following centrifugation (15,000 × *g*, 30 min), the inclusion bodies were washed twice with buffer B1 and solubilized in cleavage buffer (20 mM Tris-HCl, 500 mM NaCl, 1 mM EDTA, 40 mM DTT, pH 8.5).

The intein cleavage reaction was performed at 20 °C for 3 h, followed by an additional 12 h at 4 °C. The acid-soluble fraction was isolated by centrifugation (15,000 × *g*, 20 min), desalted on a Sephadex G-25 column (Cytiva, USA), concentrated by ultrafiltration using a 1 kDa cutoff membrane, and lyophilized. The lyophilized peptides were stored at − 80 °C. SDS-PAGE analysis was conducted using tricine gels stained with Coomassie Brilliant Blue R-250. The peptide purity was greater than 95%. The final yield of purified $Scymidgutin_{8–29}$ was 4.6 mg/g wet cell weight. Endotoxin levels in the final peptide preparation were determined using a Limulus amebocyte lysate (LAL) assay with a sensitivity of 0.06 EU/mL. Protein concentrations were determined using the BCA Protein Assay Kit (Beyotime, China) with bovine serum albumin as the standard, according to the manufacturer's instructions.

## Microbial Strains

We purchased strains from the China General Microbiological Culture Collection Center (CGMCC), including *Micrococcus luteus* (CGMCC No. 1.2299), *Micrococcus lysodeikticus* (CGMCC No. 1.634), *Corynebacterium glutamicum* (CGMCC No.1.1886), *Bacillus subtilis* (CGMCC No. 1.3358), *Staphylococcus epidermidis (*CGMCC No.*1.426)*, *Enterococcus faecium* (CGMCC No. 1.131), *Listeria monocytogenes* (CGMCC No.1.10753), *Staphylococcus aureus* (CGMCC No. 1.2465 and CGMCC No. 11.879), *Bacillus cereus* (CGMCC No.1.376), *Enterococcus faecalis* (CGMCC No.1.2135), *Pseudomonas stutzeri* (CGMCC No. 1.1803), *Acinetobacter baumannii* (CGMCC No. 1.6769), *Shigella flexneri* (CGMCC No. 1.1868), *Pseudomonas fluorescens* (CGMCC No. 1.3202), *Escherichia coli* (CGMCC No. 1.2389), *Vibrio harveyi* (CGMCC No.1.1593), *Vibrio parahaemolyticus* (CGMCC

No.1.1615), *Vibrio alginolyticus* (CGMCC No.1.1833), *Aeromonas. hydrophila* (CGMCC No. 1.2017), *Vibrio fluvialis* (CGMCC No.1.1609), *Cryptococcus neoformans* (CGMCC No.2.1563), *Fusarium oxysporum* (CGMCC No. 3.6785), *Candida tropicalis* (CGMCC No.2.1975), *Candida krusei* (CGMCC No.2.1857), *Fusarium solani* (CGMCC No. 3.584), *Fusarium graminearum* (CGMCC No. 3.4521), *Aspergillus niger* (CGMCC No. 3.316), *Aspergillus fumigatus* (CGMCC No.3.5835), *Candida parapsilosis* (CGMCC No.2.1846), and *Candida albicans* (CGMCC No.2.2411). In addition, the clinical isolates including MRSA (QZ18090, QZ19130, QZ19134), MDR *Enterococcus faecium* (QZ19139), MDR *Enterococcus faecalis* (QZ18087), MDR *Acinetobacter baumannii* (QZ18050, QZ18055, QZ20141, QZ20142, QZ20143), MDR *Escherichia coli* (QZ18109, QZ18110, QZ20149, QZ20150), and MDR *Pseudomonas aeruginosa* (QZ19121, QZ19123, QZ19125, QZ18103) were provided by the Second Affiliated Hospital of Fujian Medical University (Quanzhou, Fujian, China).

## Antimicrobial Assay

The antimicrobial activity of Scymidgutin$_{8–29}$ was assessed via a modified broth microdilution assay. Bacterial suspensions ($1.5 \times 10^6$ CFU/mL in Mueller-Hinton broth; HKM Biotechnology, China) were incubated with serial dilutions of Scymidgutin$_{8–29}$ (1.5–96 μM) in 96-well plates (NEST Scientific, China) at 37 °C for 24 h, with LL-37 (GL Biochem, China) and sterile Milli-Q® water serving as positive and negative controls, respectively. The minimum inhibitory concentration (MIC) was defined as the lowest peptide concentration inhibiting visible growth, whereas the minimum bactericidal concentration (MBC) was determined as the lowest concentration achieving ≥ 99.9% bacterial lethality. All assays were performed in triplicate (three biological replicates, each with three technical repetitions).

## Bactericidal Kinetics Analysis

Time-kill assays were conducted against *S. aureus* and *A. baumannii* according to established protocols. Mid-log phase cultures (~$1 \times 10^6$ CFU/mL in Mueller-Hinton broth) were treated with Scymidgutin$_{8–29}$ (1×MIC) at 37 °C under continuous agitation (200 rpm). Aliquots were collected at specified intervals (0, 5, 10, 15, 20, 25, 30, 45, 60, 90, 120, 150 min), serially diluted in sterile PBS, and plated on nutrient agar. Viable counts were quantified after 24 h of incubation at 37 °C, using untreated cultures as negative controls. Three biological replicates were analyzed, with triplicate plating for each time point.

## Membrane Perturbation Assay

Membrane perturbation by Scymidgutin$_{8–29}$ was evaluated using the fluorescent probe N-phenyl-1-naphthylamine (NPN; Sigma-Aldrich, USA). NPN is a hydrophobic probe that fluoresces upon partitioning into membrane environments. In NPN uptake assays, kinetic changes in fluorescence intensity rather than absolute values at individual time points were used to assess membrane perturbation, because modest baseline fluorescence variations can occur due to spontaneous probe partitioning, particularly in Gram-positive bacteria which lack an outer membrane [35]. Mid-log phase cultures of *S. aureus* and *A. baumannii* were washed with sodium phosphate buffer (NaPB; pH 7.4) and resuspended in 5 mM HEPES containing 5 mM glucose ($OD_{600} \approx 0.5$, ~$10^8$ CFU/mL). Cell suspensions were pre-incubated with 10 μM NPN in black 96-well plates for 5 min (25 °C, dark) before treatment with Scymidgutin$_{8–29}$ (24 μM), LL-37 (24 μM; GL Biochem, China), or polymyxin B (PMB; 20 μg/mL; Solarbio, China). Fluorescence intensity was measured at 2-minute intervals (excitation 350 nm, emission 420 nm) using a microplate reader (Tecan Infinite 200 Pro, Switzerland). All assays were performed with three technical replicates and repeated in three independent biological experiments.

## Cytoplasmic Membrane Integrity

Membrane integrity was assessed using the LIVE/DEAD™ BacLight™ Bacterial Viability Kit (Thermo Fisher Scientific, USA).

Bacterial suspensions of *S. aureus* CGMCC 1.2465 and *A. baumannii* CGMCC 1.6769 (~$10^7$ CFU/mL in NaPB) were incubated with Scymidgutin$_{8–29}$, LL-37 (positive control), or PMB (positive control) at the indicated concentrations for 30 min. Following PBS washing, cells were dual-stained with SYTO 9 (3.34 μM) and propidium iodide (PI; 20 μM) for 15 min in the dark. Membrane integrity was visualized by confocal laser scanning microscopy (Zeiss LSM 780, Germany) using sequential excitation at 488 nm (SYTO 9) and 561 nm (PI).

## Scanning Electron Microscopy (SEM)

Mid-log phase cultures of *S. aureus* and *A. baumannii* ($1 \times 10^8$ CFU/mL in 10 mM sodium phosphate buffer, NaPB) were incubated with Scymidgutin$_{8–29}$ (1×MIC) for 30 min at 25 °C. Following overnight fixation in 2.5% (v/v) glutaraldehyde at 4 °C, samples were washed three times with NaPB, immobilized on poly-L-lysine-coated glass coverslips, and dehydrated through a graded ethanol series (30%, 50%, 70%, 90%, and 100%). Critical point drying

was performed using a Leica EM CPD300 system (Leica Microsystems, Germany) before gold sputtering (20 nm thickness). Cellular ultrastructure was examined using a field-emission scanning electron microscope (FEI Quanta 650 FEG) operated at 5 kV accelerating voltage.

### Transmission Electron Microscopy (TEM)

Bacterial suspensions incubated with Scymidgutin$_{8–29}$ (1× MIC for 30 min) were primarily fixed in 2.5% glutaraldehyde (in 0.1 M phosphate buffer, pH 7.4), then post-fixed with 1% osmium tetroxide, and subsequently embedded in epoxy resin after agarose immobilization. Ultrathin Sect. (70 nm thickness) were double-stained with 2% uranyl acetate and Reynolds' lead citrate, then examined using a Hitachi HT7800 transmission electron microscope (Hitachi High-Tech, Japan) operated at 80 kV accelerating voltage.

### Reactive Oxygen Species (ROS) Detection

Bacterial suspensions of *S. aureus* and *A. baumannii* (approximately $1 \times 10^7$ CFU/mL in 10 mM sodium phosphate buffer, pH 7.4) were incubated with 10 μM 2',7'-dichlorodihydrofluorescein diacetate (DCFH-DA; Nanjing Jiancheng, China) for 30 min at 37 °C in the dark. After treatment with either Scymidgutin$_{8–29}$ (1×MIC) or polymyxin B (20 μg/mL; positive control), ROS production was measured by fluorescence intensity (excitation/emission: 485/525 nm) using a Tecan Infinite® M200 Pro microplate reader (Tecan Group Ltd., Switzerland). Fluorescence readings were acquired at 5-minute intervals for 60 min. The experiment was performed with three independent biological replicates, each containing triplicate technical measurements.

### Extracellular ATP Quantification

Bacterial suspensions ($1 \times 10^7$ CFU/mL) that had been treated with Scymidgutin$_{8–29}$ were centrifuged (12,000×g, 4 °C, 10 min). The supernatants were analyzed using the ATP Determination Kit (Thermo Fisher Scientific, USA) according to the manufacturer's protocol. Bioluminescence signals (560 nm) were measured using a GloMax® 20/20 luminometer (Promega, USA) and normalized against an ATP standard curve. All assays were performed in triplicate with at least three independent repetitions.

### Competitive Inhibition Assay using Bacterial Surface Components

Lipoteichoic acid (LTA; *S. aureus*-derived, Sigma-Aldrich, USA) or LPS (*E. coli*, Sigma-Aldrich, USA) was serially diluted (8–64 μg/mL) in 96-well plates and pre-incubated with Scymidgutin$_{8–29}$ (1×MIC) for 30 min at 25 °C. Bacterial suspensions (*S. aureus* or *A. baumannii*; $5 \times 10^5$ CFU/mL in Mueller-Hinton broth) were added to inhibitor-peptide complexes and incubated at 37 °C for 24 h. Bacterial growth inhibition was quantified by measuring optical density at 595 nm using a Tecan Infinite® M200 Pro microplate reader (Tecan Group Ltd., Switzerland). All assays were performed with three independent biological replicates, each containing triplicate technical measurements.

### Isothermal Titration Calorimetry (ITC)

The direct binding affinity between Scymidgutin$_{8–29}$ and bacterial surface components (LPS from *E. coli* and LTA from *S. aureus*) was measured using a MicroCal PEAQ-ITC instrument (Malvern Panalytical, UK). All solutions were degassed and equilibrated at 25 °C prior to measurements. Scymidgutin$_{8–29}$ (200 μM) was titrated into the sample cell containing LPS or LTA (200 μM) in HEPES buffer (pH 7.4) with 19 injections of 2 μL each at 150-s intervals. Control experiments were performed by titrating the peptide into buffer alone to correct for dilution heat. The binding isotherms were analyzed using MicroCal PEAQ-ITC Analysis Software. The LPS data were fitted to a two-site binding model, while the LTA data were fitted to a one-site binding model. Data are presented as enthalpy change (ΔH) versus molar ratio [peptide]/[LPS or LTA].

### Thermal Stability Profiling

The thermostability of Scymidgutin$_{8–29}$ was assessed against *S. aureus* and *A. baumannii* using sequential thermal challenges. Mid-log phase cultures ($1 \times 10^7$ CFU/mL) were co-incubated with scymidgutin$_{8–29}$ solution at 4–121 °C and heated for 120 min. Post-treatment samples were equilibrated to 25 °C before co-culturing with bacterial suspensions in 96-well plates (37 °C, 18 h). The retention of antimicrobial activity was quantified by measuring $OD_{600}$. All experiments were performed in triplicate with at least three biological replicates.

### Cytotoxicity and Hemolysis Assay

HEK-293T, RAW 264.7, and ZF4 cells were seeded at a density of $1 \times 10^4$ cells/well in 96-well plates. After 24 h incubation with Scymidgutin$_{8–29}$ (3–48 μM), cellular metabolic activity was assessed using the CellTiter 96® AQueous MTS Reagent (Promega, USA) according to the manufacturer's instructions. The absorbance was measured at 490 nm, with background subtraction performed at 650 nm. Murine erythrocytes (C57BL/6 strain, 4% hematocrit in PBS) were incubated with Scymidgutin$_{8–29}$ (3–96 μM) for

1 h at 37 °C. Following centrifugation (500 × g, 5 min), hemoglobin release was determined by measuring supernatant absorbance at 540 nm. Triton X-100 (1%) and PBS were used as positive and negative controls, respectively. All assays included three biological replicates with quadruplicate technical repeats.

## Immunofluorescence Staining

RAW 264.7 cells were seeded at a density of $2 \times 10^5$ cells/well in 12-well plates and treated with $Scymidgutin_{8–29}$ in the presence or absence of 1 μg/mL lipopolysaccharide (LPS) for 24 h. Following treatment, cells were fixed with 4% paraformaldehyde (30 min), permeabilized with 0.1% Triton X-100 in PBS (10 min), and blocked with 3% BSA (1 h, RT). For M1 macrophage identification, samples were incubated with anti-iNOS primary antibody (1:200 dilution, 4 °C, overnight) followed by CY3-conjugated goat anti-rabbit IgG secondary antibody (1:500 dilution, 1 h, RT). For M2 polarization analysis, parallel samples were incubated with anti-Arg-1 primary antibody (1:200 dilution) and DyLight 488-conjugated secondary antibody (1:500 dilution) under identical conditions. After three washes with PBS, all samples were counterstained with DAPI (1 μg/mL, 5 min). Fluorescence images were captured using an inverted fluorescence microscope (Zeiss, Germany). For macrophage assays, the positive control, 5-aminosalicylic acid (5-ASA; Sigma-Aldrich, USA) was dissolved in DMSO (final concentration 0.1% v/v) and used at a working concentration of 1 mM.

For quantitative analysis, the mean fluorescence intensity of iNOS and Arg-1 staining was measured from five randomly selected fields per sample using ImageJ software (NIH, USA). Background fluorescence was subtracted, and the values were normalized to the number of DAPI-stained nuclei in each field. Data were expressed as mean fluorescence intensity ± SEM from three independent experiments.

## NO Secretion Assay in LPS-stimulated RAW 264.7 Macrophages

RAW 264.7 murine macrophages were maintained in DMEM supplemented with 10% FBS at 37 °C in a humidified 5% $CO_2$ atmosphere. Cells were seeded in 96-well plates at a density of $1 \times 10^6$ cells/mL (100 μL/well) and allowed to adhere for 2 h. The medium was replaced with fresh DMEM containing 1 μg/mL LPS (*E. coli* O111, Sigma-Aldrich, USA) or vehicle control. Following 18 h incubation, nitric oxide (NO) levels in culture supernatants were determined using the Griess reaction system (Beyotime, China) by measuring absorbance at 540 nm with a microplate reader, using sodium nitrite standards for calibration. All experiments were performed in triplicate with at least three independent biological replicates.

## Zebrafish Caudal Fin Wound Model Establishment

Zebrafish larvae at 3 dpf were anesthetized using 0.02% (w/v) MS-222 (Sigma-Aldrich, USA) dissolved in E3 embryo medium. Under stereomicroscopic observation, tail fin amputation was performed with a sterile 1-mm scalpel blade on 2% agarose-coated Petri dishes to minimize trauma to the notochord and surrounding tissues. Following amputation, larvae were immediately transferred to fresh E3 medium and maintained at 28.0 ± 0.5 °C under standard culture conditions. Neutrophil recruitment to the wound site was quantified by fluorescence microscopy at 6 hpa. Neutrophil recruitment to the wound site was quantified by measuring the mean fluorescence intensity within a defined region of interest (ROI) encompassing the wound area using ImageJ software (NIH, USA). Background fluorescence was subtracted from an identically sized ROI in an uninjured region.

## Establishment of LPS/DSS-induced Inflammation Models in Zebrafish

3 dpf zebrafish larvae maintained in E3 medium under standard conditions (28.0 ± 0.5 °C) were treated with either LPS (10 μg/mL) or dextran sulfate sodium (DSS; 3% w/v) for 40 min. Following treatment, specimens were immediately subjected to fluorescence microscopy imaging (Zeiss Axio Observer, Germany) to analyze neutrophil spatial distribution patterns in intact tissue architecture. Neutrophil accumulation in the hindbrain region was quantified by measuring the mean fluorescence intensity within a standardized ROI using ImageJ software; background subtraction was performed as described above.

## Therapeutic Evaluation in IBD Models

Female C57BL/6 mice (6–8 weeks old, GemPharmatech Co., Ltd.) were housed under specific pathogen-free conditions (21 ± 1 °C, 40–70% relative humidity, 12 h light/dark cycle) with ad libitum access to food and water. After one week of acclimation, the mice were randomly allocated into four groups ($n$ = 10 per group) using stratified randomization by body weight to ensure comparable baseline weights across groups: (i) normal control (PBS), (ii) DSS model, (iii) $Scymidgutin_{8–29}$ treatment (5 mg/kg), and (iv) positive control 5-ASA (30 mg/kg). Colitis was induced by administering 3% (w/v) dextran sulfate sodium (DSS, 36–50 kDa; Yeasen Biotechnology, China) in drinking water ad libitum for 7 consecutive days.

Treatments were administered intrarectally at 24 h intervals in a volume of 100 µL using a 22-gauge soft catheter inserted 3 cm into the rectum; no anesthesia was required for this procedure. The dose of Scymidgutin$_{8-29}$ (5 mg/kg) was selected based on a pilot dose-ranging experiment (2.5, 5, and 10 mg/kg) in DSS-treated mice, while the dose of 5-ASA (30 mg/kg) was chosen according to published effective doses for intrarectal administration in murine colitis models [36].

The Disease Activity Index (DAI) was assessed daily by three independent investigators blinded to group allocation. The DAI was calculated as the average of three subscores: (i) body weight loss (0, none; 1, 1–5%; 2, 5–10%; 3, 10–20%; 4, >20%), (ii) stool consistency (0, normal; 2, loose stools; 4, diarrhea), and (iii) fecal blood (0, negative; 2, positive; 4, gross bleeding). Exclusion criteria were defined as >5% body weight loss at baseline or overt rectal bleeding prior to DSS administration; no mice met these criteria. On day 7, the mice were euthanized by cervical dislocation, and colon tissues and fecal samples were collected for subsequent analyses.

All animal experiments were approved by the Institutional Animal Care and Use Committee (IACUC) of Xiamen University (Approval No. XMULAC20240082) and were conducted in accordance with the relevant guidelines.

## Histopathological Evaluation

Distal colon segments (approximately 3 cm proximal to the anus, where DSS-induced injury is most severe) were fixed in 4% (w/v) paraformaldehyde (pH 7.4) for 24 h at 4 °C, processed through ethanol-xylene gradients, and embedded in paraffin using the Swiss-roll technique. Serial Sect. (5 µm) were stained with hematoxylin/eosin (H&E) and imaged under a Leica microscope (Leica DMi1, Germany). Histopathological scoring was performed in a blinded manner by three independent investigators unaware of group allocation. For each colon section, four parameters were scored on a 0–4 scale: (i) epithelial damage (0: none; 1: focal thinning; 2: multifocal erosion; 3: extensive ulceration involving < 50% of the epithelial surface; 4: widespread ulceration involving > 50%), (ii) inflammatory infiltration (0: none; 1: mild, limited to the mucosa; 2: moderate, extending to the submucosa; 3: severe transmural infiltration; 4: extremely severe with crypt abscesses), and (iii) crypt destruction (0, intact architecture; 1, focal crypt elongation or dilation; 2, multifocal crypt loss < 25%; 3, extensive crypt loss 25–50%; 4, nearly complete crypt loss > 50%), Three non-overlapping fields were evaluated per section, and the scores were averaged. The total histological score (range, 0–12) was calculated as the sum of the three individual parameter scores.

## Cytokine Profiling

Colon tissues were homogenized in ice-cold PBS containing: Collagenase I (2 mg/mL; Solarbio, China), Collagenase IV (1.5 mg/mL; Solarbio, China), Hyaluronidase (1 mg/mL; Solarbio, China). Supernatants were collected after centrifugation (12,000 × g, 15 min, 4 °C) and analyzed via ELISA for: IL-1β (A00101; Boster, China), TNF-α (BA0131; Boster, China), IL-6 (A00102-2; Boster, China), IL-10 (A00021-2; Boster, China).

## Gut Microbiota 16 S rRNA Sequencing

Fresh fecal pellets from C57BL/6 mice ($n = 10$ per group) were flash-frozen in liquid nitrogen and stored at −80 °C until processing. Samples were homogenized in 1 mL of sterile PBS by vigorous vortexing. Genomic DNA was extracted using the QIAamp Fast DNA Stool Mini Kit (Qiagen) following the manufacturer's protocol, with purity assessed via NanoDrop spectrophotometry. DNA integrity was verified by 1% agarose gel electrophoresis. The V4 hypervariable region of the 16 S rRNA gene was amplified with barcoded primers 515 F and 806R. Amplicons were purified using AMPure XP beads (Beckman Colter, USA), quantified by qPCR (KAPA Library Quantification Kit), and pooled. Libraries were sequenced on an Illumina NovaSeq 6000 platform (Novogene) with 250-bp paired-end reads. Raw sequences were processed in QIIME2 (v2020.11): demultiplexed, quality-filtered (max expected errors = 1.0), and denoised using DADA2. Taxonomy was assigned against the SILVA 138 database (99% similarity threshold). All samples were rarefied to 30,000 sequences before analysis. Alpha diversity indices (Shannon and Chao1) were calculated, and beta diversity was evaluated using weighted and unweighted UniFrac distances with principal coordinate analysis (PCoA) for visualization.

## Statistical Analysis

All data are presented as mean ± standard error of the mean (SEM) from at least three independent experiments. Statistical significance was determined using GraphPad Prism 8 software. Comparisons between two groups were analyzed using an unpaired two-tailed Student's t-test. Multiple group comparisons were performed using one-way analysis of variance (ANOVA) followed by Tukey's post-hoc test. A $p$-value of less than 0.05 was considered statistically significant.

## Results

### Design and Characterization of the Core Peptide Scymidgutin$_{8–29}$

Using the mud crab transcriptome database established in our laboratory, we amplified a novel gene using RACE-PCR. The full-length cDNA contained a 97 bp 5' UTR, 99 bp 3' UTR, and a 204 bp open reading frame encoding a 67-amino-acid protein (Fig. 1A, B). Tissue-specific expression profiling by qPCR demonstrated predominant transcript accumulation in adult midgut tissues of both sexes, leading to its designation as Scymidgutin (Fig. S1A, B). Developmental stage analysis further revealed ubiquitous expression across the mud crab development stages (Fig. S1C). The encoded cationic protein exhibited a calculated molecular weight of 7.62 kDa and theoretical isoelectric point (pI) of 11.38 (Table 1). Using the CAMPR3 antimicrobial peptide database, we designed Scymidgutin$_{8–29}$, a truncated peptide spanning residues$_{8–29}$ of the mature Scymidgutin protein (Fig. 1C, D, E) and documented its sequence with key physicochemical characteristics (Table 2). This 22-residue peptide had a calculated molecular mass of 2658.23 Da, 37.5% hydrophobicity, and an estimated pI of 12.31. This peptide was successfully produced using a recombinant fusion system for subsequent studies. The purity and molecular mass of the recombinant Scymidgutin$_{8–29}$ peptide were confirmed by Tricine-SDS-PAGE and reversed-phase HPLC (Fig. S2). The final yield of purified recombinant Scymidgutin$_{8–29}$ was 4.6 mg/g wet cell weight. Endotoxin levels in the final peptide preparation were determined using a Limulus amebocyte lysate (LAL) assay with a sensitivity of 0.06 EU/mL and were below the detection limit (<0.06 EU/mL), confirming that the peptide preparation was suitable for in vivo administration.

### Evaluation of Antimicrobial Activity

The antimicrobial activities of Scymidgutin$_{8–29}$ were examined using a series of microbial strains. The results showed that Scymidgutin$_{8–29}$ has broad-spectrum activity. The MIC and MBC values determined in the experiment are detailed in Table 3. The truncated peptide Scymidgutin$_{8–29}$ demonstrated differential antimicrobial efficacy against clinically relevant pathogens and gut-associated strains. Against nosocomial pathogens, *A. baumannii* (MIC < 1.5 μM; MBC 1.5–3 μM) and *S. aureus* (MIC 3–6 μM; MBC 6–12 μM) exhibited sensitivity, while the opportunistic fungal pathogen *Candida albicans* required higher inhibitory concentrations (MIC 6–12 μM; MFC > 48 μM). Notably, intestinal commensals and enteric pathogens displayed variable susceptibility: *Enterococcus faecium* (MIC 1.5–3 μM) and *Shigella flexneri* (MIC < 1.5 μM) were inhibited at low micromolar ranges, as well as *E. coli* (MIC 6–12 μM) and *Enterococcus faecalis* (MIC 24–48 μM) at higher concentrations. In addition, Scymidgutin$_{8–29}$ exhibits potent antimicrobial activity against clinical isolates, demonstrating strong antimicrobial activity against MRSA and multidrug-resistant *A. baumannii*, with minimum inhibitory concentration (MIC) values ranging from 1.5 to 24 μM and minimum bactericidal concentration (MBC) values ranging from 1.5 to 24 μM (Table 4).

### Bactericidal Kinetics and Stability of Scymidgutin$_{8–29}$

Bactericidal kinetics assessment revealed that Scymidgutin$_{8–29}$ has rapid eradication capacity against *A. baumannii* and *S. aureus*, achieving 1×MBC thresholds within 15 min and 20 min, respectively, with >99.9% viability reduction (Fig. 2A, B). The thermal stability of Scymidgutin$_{8–29}$ was evaluated through continuous thermal shock experiments. The results indicated that Scymidgutin$_{8–29}$ had bactericidal efficacy against both *A. baumannii* and *S. aureus*. After being exposed to 4–121 °C for 2 h and then co-incubated with bacteria for 24 h, the peptide maintained approximately 99% of its antibacterial effect (Figs. 2C, D), confirming exceptional thermostability.

We further evaluated the stability of Scymidgutin$_{8–29}$ in simulated gastrointestinal fluids. The peptide (1×MBC) was incubated in simulated gastric fluid (SGF, pH 2.0, containing pepsin) and simulated intestinal fluid (SIF, pH 6.8, containing trypsin) at 37 °C for up to 4 h, and residual antibacterial activity against *A. baumannii* and *S. aureus* was assessed at various time points. In SIF, the peptide retained full antibacterial activity for up to 2 h, but activity was lost after 4 h of incubation. In SGF (pH 2.0), the peptide maintained activity for 1 h, but was inactivated after 2 and 4 h (Figs. 2E, F).

### Antimicrobial Mechanism of Scymidgutin$_{8–29}$

The membrane-disruptive effect of Scymidgutin$_{8–29}$ was initially assessed through N-phenyl-1-naphthylamine (NPN) uptake assays. Figure 2G‒H demonstrates concentration-dependent fluorescence enhancement in both *A. baumannii* and *S. aureus* following treatment. In *A. baumannii*, the increase in NPN fluorescence indicated outer membrane permeabilization, as NPN partitions into the hydrophobic core of the damaged outer membrane. In *S. aureus*, which lacks an outer membrane, the enhanced NPN signal reflected disruption of the cytoplasmic membrane, allowing the probe to access the hydrophobic interior of the phospholipid bilayer.

A

```
1                    TAATATTGTATTTACTCTTCCCCGACATTTTTGCTGGGTTAGTGCAAAA
50   GTCGCCGTCTTCCTAATTCTTGGCGAGGGTTCCCGCTGCGTGCAGACGATGACACGGGAC
1                                                    M  T  R  D
110  GCCCTAGAGTTACCTTGGACACGCCTACACTCTAAAAAGCGGGGTGTGCTCCTCCGTCTT
5     A  L  E  L  P  W  T  R  L  H  S  K  K  R  G  V  L  L  R  L
170  CAACTCTCACAGAAGGCCGGGGAGGAGGTGGCGGTGTCCAGGCGTGGTCGTGTCTCACTG
25    Q  L  S  Q  K  A  G  E  E  V  A  V  S  R  R  G  R  V  S  L
230  GAAACTCTTGGTGAGAGCCCAGTGAGGAGGGAAGCACCAAGTGAAGGGTGGAGGCGTGTG
45    E  T  L  G  E  S  P  V  R  R  E  A  P  S  E  G  W  R  R  V
190  CAGGGTGTGTAGATGACACGGGACGCCCTAGAGTTACCTTGGACACGCCTACACTCTAAA
65    Q  G  V  *
350  AAGCGGGGTGTGCTCCAAAAAAAAAAAAAAAAAAAAAAAAAAAAAAAAAAAAAAAAAA
```

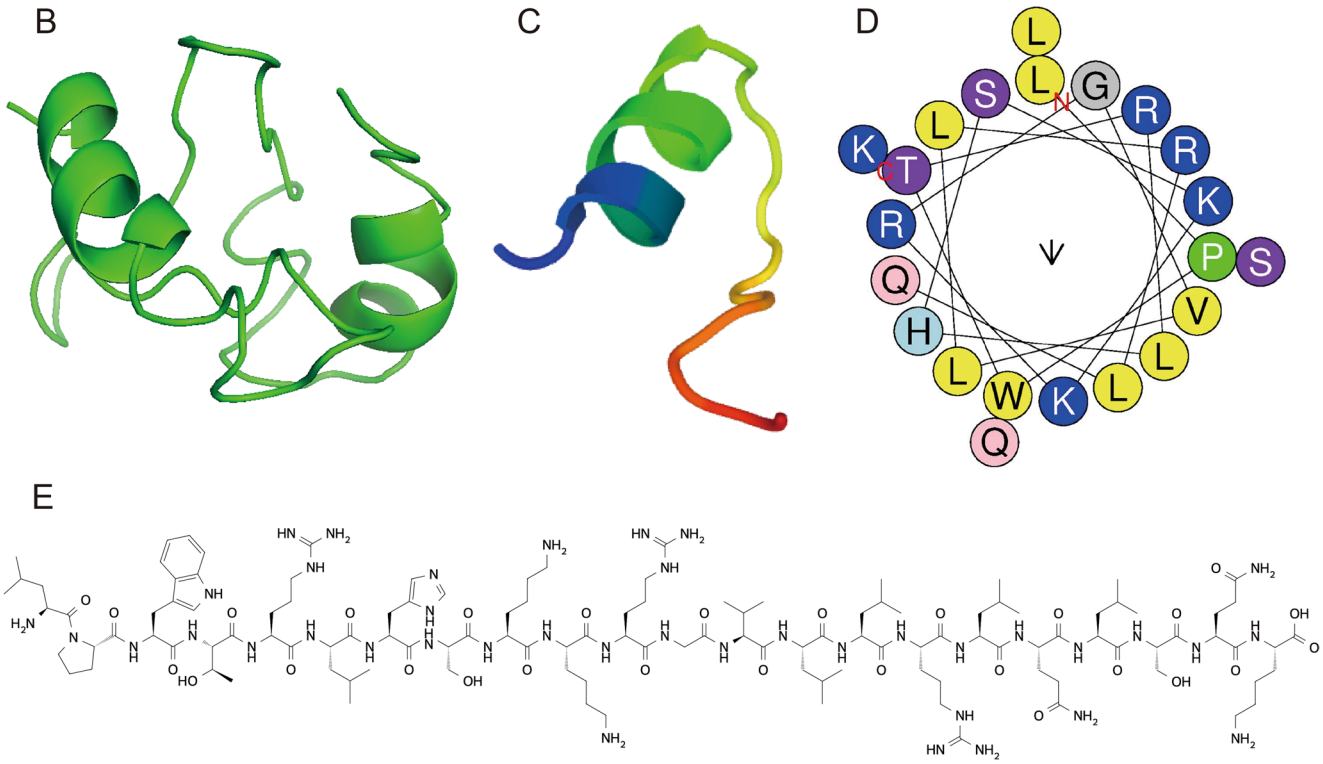



**Fig. 1** Molecular characterization and expression profiling of Scymidgutin in *S. paramamosain*. (**A**) Full-length cDNA sequence and deduced amino acid sequence. The red box indicates the Scymidgutin$_{8\text{-}29}$ core peptide. (**B**) Predicted three-dimensional structure of the full-length protein. (**C**) Predicted three-dimensional structure of the Scymidgutin$_{8\text{-}29}$ peptide. (**D**) Helical wheel projection of Scymidgutin$_{8\text{-}29}$. (**E**) Chemical structure of Scymidgutin$_{8\text{-}29}$

Subsequent dual staining with SYTO 9 and propidium iodide (PI) revealed differential membrane integrity: while SYTO 9 uniformly labeled all bacterial cells, PI infiltration specifically marked inner membrane-compromised populations (Fig. 2I, J).

Confocal microscopy analysis of *A. baumannii* and *S. aureus* showed that the PI signal was significantly enhanced in the Scymidgutin$_{8\text{–}29}$-treated specimens, with a nearly complete shift from green to red fluorophores in both

**Table 1** Sequence information and physicochemical properties of Scymidgutin

| Physicochemical parameters | Scymidgutin |
|---|---|
| Number of amino acids | 67 |
| Molecular MW (Da) | 7620.77 |
| Theoretical PI | 11.38 |
| Formula | $C_{329}H_{556}N_{110}O_{96}S_1$ |
| Total number of atoms | 1092 |
| Grand average of hydropathicity | −0.688 |

**Table 2** The key physicochemical parameters of Scymidgutin$_{8–29}$

| Physicochemical parameters | Scymidgutin$_{8–29}$ |
|---|---|
| Sequence | LPWTRLHSKKRGVLLRLQLSQK |
| Number of amino acids | 22 |
| Molecular MW (Da) | 2658.23 |
| Theoretical PI | 12.31 |
| Formula | $C_{121}H_{209}N_{39}O_{28}$ |
| Hydrophobic residue% | 37.5% |
| Hydrophobic moment | 0.146 |
| Grand average of hydropathicity | −0.618 |
| Total net charge | +6 |

stains, suggesting extensive disruption of the cytoplasmic membrane. Scanning and transmission electron microscopy (SEM/TEM) revealed structural disintegration of cell membranes in Scymidgutin$_{8–29}$-treated *A. baumannii* and *S. aureus*, accompanied by cytoplasmic extrusion (Fig. 3A, B). In untreated controls, cellular envelopes retained intact structural continuity with preserved membrane architecture.

The antimicrobial mechanism was further investigated through ROS-mediated oxidative stress potentiation. Quantification of reactive oxygen species (ROS) in *A. baumannii* and *S. aureus* following Scymidgutin$_{8–29}$ exposure revealed concentration-dependent intracellular radical accumulation (Fig. 3C, D). Parallel assessment of extracellular ATP levels demonstrated dose-responsive efflux kinetics, with significant ATP release detected within 30 min post-treatment (Fig. 3E, F), indicative of comprehensive membrane barrier collapse.

The antimicrobial activity of Scymidgutin$_{8–29}$ was competitively attenuated by bacterial surface components, with LPS and LTA exhibiting dose-dependent neutralization against its Gram-positive and Gram-negative targeting, respectively. Exogenous supplementation of LPS (8–64 μg/mL) reduced Scymidgutin$_{8–29}$-mediated killing efficacy in *A. baumannii* (Fig. 4A), while parallel LTA administration (64 μg/mL) similarly compromised bactericidal effects against *S. aureus* (Fig. 4B). This concentration-dependent inhibition pattern suggests that exogenous LPS and LTA competitively interfere with the interaction between Scymidgutin$_{8–29}$ and its bacterial surface targets, thereby attenuating its antibacterial activity.To directly evaluate the binding capacity of Scymidgutin$_{8–29}$ to bacterial surface components, we performed ITC. As shown in Fig. 4C-F, titration of the peptide into LPS produced a biphasic heat profile with negative peaks in the early injections and positive deflections at later stages, indicative of multiple binding events. The LPS data were best fitted to a two-site binding model: a lower-affinity site ($Kd_1$ = 1.93 μM, $N_1$ = 0.86, $\Delta H_1$ = −24.5 kJ/mol) and a higher-affinity site ($Kd_2$ = 28.6 nM, $N_2$ = 0.49, $\Delta H_2$ = +11.0 kJ/mol). The negative ΔH for Site 1 suggests enthalpically driven interactions (e.g., electrostatic/hydrogen bonds), whereas the positive ΔH for Site 2 indicates an entropy-driven process (e.g., hydrophobic insertion and aggregate disruption). In contrast, titration into LTA yielded a canonical exothermic isotherm that was adequately fitted to a one-site model, with Kd = 689 nM, $N$ = 1.20, ΔH = −32.0 kJ/mol, and ΔG = −35.2 kJ/mol, confirming a favorable enthalpic interaction. Collectively, these ITC results confirm that Scymidgutin$_{8–29}$ directly binds to both LPS and LTA, supporting the competitive inhibition data and demonstrating that its antibacterial activity involves direct targeting of bacterial surface components.

## Scymidgutin$_{8–29}$ Shows Anti-inflammatory Activity and No Cytotoxicity

The cytotoxic potential of Scymidgutin$_{8–29}$ was assessed in HEK-293T, RAW 264.7, and ZF4 cell lines. No cytotoxicity was observed in normal zebrafish and mammalian cell models (Fig. 5A-C). Subsequent evaluation of hemolytic activity in murine erythrocytes demonstrated the absence of hemolytic response across 3–96 μM concentrations (Fig. 5D). Collectively, these results demonstrate the biocompatibility of Scymidgutin$_{8–29}$.

**Table 3** Antimicrobial activities of Scymidgutin$_{8–29}$

| Microorganisms | CGMCC No.[a] | MIC[b] (μM) | MBC[c]/MFC[d] (μM) |
|---|---|---|---|
| Gram-positive bacteria | | | |
| *Micrococcus luteus* | 1.2299 | < 1.5 | < 1.5 |
| *Micrococcus lysodeikticus* | 1.634 | < 1.5 | < 1.5 |
| *Corynebacterium glutamicum* | 1.1886 | < 1.5 | < 1.5 |
| *Bacillus subtilis* | 1.3358 | < 1.5 | < 1.5 |
| *Staphylococcus epidermidis* | 1.426 | 1.5–3 | 1.5–3 |
| *Enterococcus faecium* | 1.131 | 1.5–3 | 1.5–3 |
| *Listeria Listeria monocytogenes* | 1.10753 | 3–6 | 3–6 |
| *Staphylococcus aureus* | 1.2465 | 3–6 | 6–12 |
| *Staphylococcus aureus* | 1.879 | 3–6 | 6–12 |
| *Bacillus cereus* | 1.376 | 6–12 | 12–24 |
| *Enterococcus faecalis* | 1.2135 | 24–48 | 24–48 |
| Gram-negative bacteria | | | |
| *Pseudomonas stutzeri* | 1.1803 | < 1.5 | 1.5–3 |
| *Acinetobacter baumannii* | 1.6769 | < 1.5 | 1.5–3 |
| *Shigella flexneri* | 1.1868 | < 1.5 | 1.5–3 |
| *Pseudomonas hydrophila* | 1.2421 | 3–6 | 12–24 |
| *Escherichia coli* | 1.2389 | 6–12 | 6–12 |
| *Vibrio harveyi* | 1.1593 | 6–12 | 6–12 |
| *Vibrio parahaemolyticus* | 1.1615 | 6–12 | 12–24 |
| *Vibrio alginolyticus* | 1.1833 | 6–12 | 12–24 |
| *Edwardsiella tarda* | | 12–24 | 24–48 |
| *Pseudomonas fluorescens* | 1.3202 | 12–24 | 24–48 |
| *Aeromonas hydrophila* | 1.2017 | 12–24 | 24–48 |
| *Vibrio fluvialis* | 1.1609 | 24–48 | > 48 |
| Fungi | | | |
| *Cryptococcus neoformans* | 2.1563 | < 1.5 | < 1.5 |
| *Fusarium oxysporum* | 3.6785 | 1.5–3 | 1.5–3 |
| *Candida tropicalis* | 2.1975 | 1.5–3 | 1.5–3 |
| *Candida krusei* | 2.1857 | 1.5–3 | 6–12 |
| *Fusarium solani* | 3.584 | 1.5–3 | 6–12 |
| *Fusarium graminearum* | 3.4521 | 3–6 | 3–6 |
| *Pichia pastoris* | | 3–6 | 6–12 |
| *Aspergillus niger* | 3.316 | 3–6 | 6–12 |
| *Aspergillus fumigatus* | 3.5835 | 3–6 | 12–24 |
| *Candida parapsilosis* | 2.1846 | 3–6 | 24–48 |
| *Candida albicans* | 2.2411 | 6–12 | > 48 |

[a] China General Microbiological Culture Collection Center

[b] The values of MIC were expressed as the interval [a]-[b]. [a] was the highest concentration tested with visible microbial growth, whereas [b] was determined as the lowest concentration without visible microbial growth

[c] The values of MBC presented are those wherein the peptide concentration killed 99.99% of the bacteria

[d] The values of MFC presented are those wherein the peptide concentration killed 99.99% of the fungi

Confocal microscopy was employed to assess macrophage polarization markers in LPS-stimulated RAW264.7 cells. LPS treatment significantly enhanced the fluorescence intensity of the M1 polarization marker iNOS while reducing the M2 marker Arg-1; both effects were reversed by Scymidgutin$_{8–29}$ administration (Fig. 5E, F). Quantification of immunofluorescence images revealed that Scymidgutin$_{8–29}$ treatment significantly reduced the mean fluorescence intensity of iNOS staining (from 4.70 ± 0.16 to 1.14 ± 0.08, $p < 0.001$) and increased the mean fluorescence intensity of Arg-1 staining (from 2.95 ± 0.14 to 5.32 ± 0.23, $p < 0.01$) compared with the LPS-stimulated group (Fig. 5G, H). ELISA quantification revealed that LPS induction markedly elevated pro-inflammatory mediators (NO, IL-6, TNF-α, IL-1β; $p < 0.01$) and suppressed anti-inflammatory IL-10 in cellular supernatants (Fig. 5I-M). Compared with the LPS-induced model group, Scymidgutin$_{8–29}$ treatment significantly attenuated pro-inflammatory cytokine levels

**Table 4** Antimicrobial activity of Scymidgutin$_{8–29}$ against clinically isolated drug-resistant bacteria

| Microorganisms | No.[a] | MIC[b] (μM) | MBC[c] (μM) |
|---|---|---|---|
| Gram-positive bacteria | | | |
| *Staphylococcus aureus* | QZ18090 | 6–12 | 6–12 |
| *Staphylococcus aureus* | QZ19130 | 12–24 | 12–24 |
| *Staphylococcus aureus* | QZ19134 | 6–12 | 6–12 |
| *Enterococcus faecium* | QZ19139 | 24–48 | 24–48 |
| *Enterococcus faecalis* | QZ18087 | 1.5–3 | 1.5–3 |
| Gram-negative bacteria | | | |
| *Acinetobacter baumannii* | QZ18050 | 3–6 | 3–6 |
| *Acinetobacter baumannii* | QZ18055 | 3–6 | 3–6 |
| *Acinetobacter baumannii* | QZ20141 | 1.5–3 | 1.5–3 |
| *Acinetobacter baumannii* | QZ20142 | 3–6 | 3–6 |
| *Acinetobacter baumannii* | QZ20143 | 6–12 | 6–12 |
| *Escherichia coli* | QZ18109 | 3–6 | 3–6 |
| *Escherichia coli* | QZ18110 | 12–24 | 12–24 |
| *Escherichia coli* | QZ20149 | 6–12 | 6–12 |
| *Escherichia coli* | QZ20150 | 6–12 | 6–12 |
| *Pseudomonas aeruginosa* | QZ19121 | 12–24 | 12–24 |
| *Pseudomonas aeruginosa* | QZ19123 | 24–48 | 24–48 |
| *Pseudomonas aeruginosa* | QZ19125 | 24–48 | 24–48 |
| *Pseudomonas aeruginosa* | QZ18103 | 12–24 | 12–24 |

[a] The Second Affiliated Hospital of Fujian Medical University (Quanzhou, Fujian, China)

[b] The values of MIC were expressed as the interval [a]-[b]. [a] was the highest concentration tested with visible microbial growth, whereas [b] was determined as the lowest concentration without visible microbial growth

[c] The values of MBC presented are those wherein the peptide concentration killed 99.99% of the bacteria

while elevating IL-10 production. These data demonstrate Scymidgutin$_{8–29}$'s significant anti-inflammatory capacity through coordinated cytokine modulation in macrophages.

We assessed the anti-inflammatory effects of Scymidgutin$_{8–29}$ in transgenic Tg (lyz: DsRed) zebrafish larvae using three distinct inflammatory models. In LPS/DSS immersion-induced inflammation, Scymidgutin$_{8–29}$ significantly suppressed inflammatory cell migration to the hindbrain region (Fig. 6A, C). Following caudal fin transection in 3 days post-fertilization (dpf) larvae, extensive neutrophil recruitment occurred at the injury site within 6 h; this chemotactic response was markedly attenuated by Scymidgutin$_{8–29}$ treatment (Fig. 6E). Quantitative analysis of fluorescence images confirmed these observations. In the LPS immersion model, Scymidgutin$_{8–29}$ treatment significantly reduced neutrophil fluorescence intensity in the hindbrain region compared with the untreated LPS group ($2.63 \pm 0.21$ vs. $1.55 \pm 0.02$ arbitrary units, $p < 0.001$; Fig. 6B). Similarly, in the DSS exposure model, neutrophil accumulation was significantly attenuated by Scymidgutin$_{8–29}$ ($2.43 \pm 0.1$ vs. $1.54 \pm 0.05$, $p < 0.001$; Fig. 6D). In the tail fin transection model, the mean fluorescence intensity at the wound site was significantly lower in Scymidgutin$_{8–29}$-treated larvae than in vehicle-treated controls at 6 h post-amputation ($2.55 \pm 0.29$ vs. $1.31 \pm 0.21$, $p < 0.01$; Fig. 6F). Consistent attenuation of inflammation-driven neutrophil trafficking across multiple models establishes the capacity of Scymidgutin$_{8–29}$ to inhibit neutrophil chemotaxis in vivo.

## Therapeutic Activity of Scymidgutin$_{8–29}$ against DSS-induced Murine IBD

A pilot dose-ranging experiment (2.5, 5, and 10 mg/kg) was performed to select the optimal dose, and 5 mg/kg was chosen based on its consistent efficacy in alleviating DSS-induced colitis (Fig. S3). Histopathological assessment revealed no detectable toxicity in mice following intrarectal administration of Scymidgutin$_{8–29}$ (5 mg/kg). Heart, liver, spleen, lung, and kidney tissues exhibited histological features comparable to PBS controls (Fig. 7A). To evaluate therapeutic potential for IBD, we employed a dextran sulfate sodium (DSS)-induced murine model. C57BL/6 mice treated with 3% (w/v) DSS developed characteristic IBD manifestations, including significant body weight loss, elevated disease activity index (DAI), and colon shortening relative to vehicle controls (PBS-treated) (Fig. 7B–F). Crucially, intrarectal delivery of Scymidgutin$_{8–29}$ (5 mg/kg) significantly attenuated DSS-induced pathophysiology, demonstrating therapeutic efficacy.

Histopathological evaluation revealed that Scymidgutin$_{8–29}$ treatment significantly restored colonic epithelial architecture and reduced inflammatory infiltrate

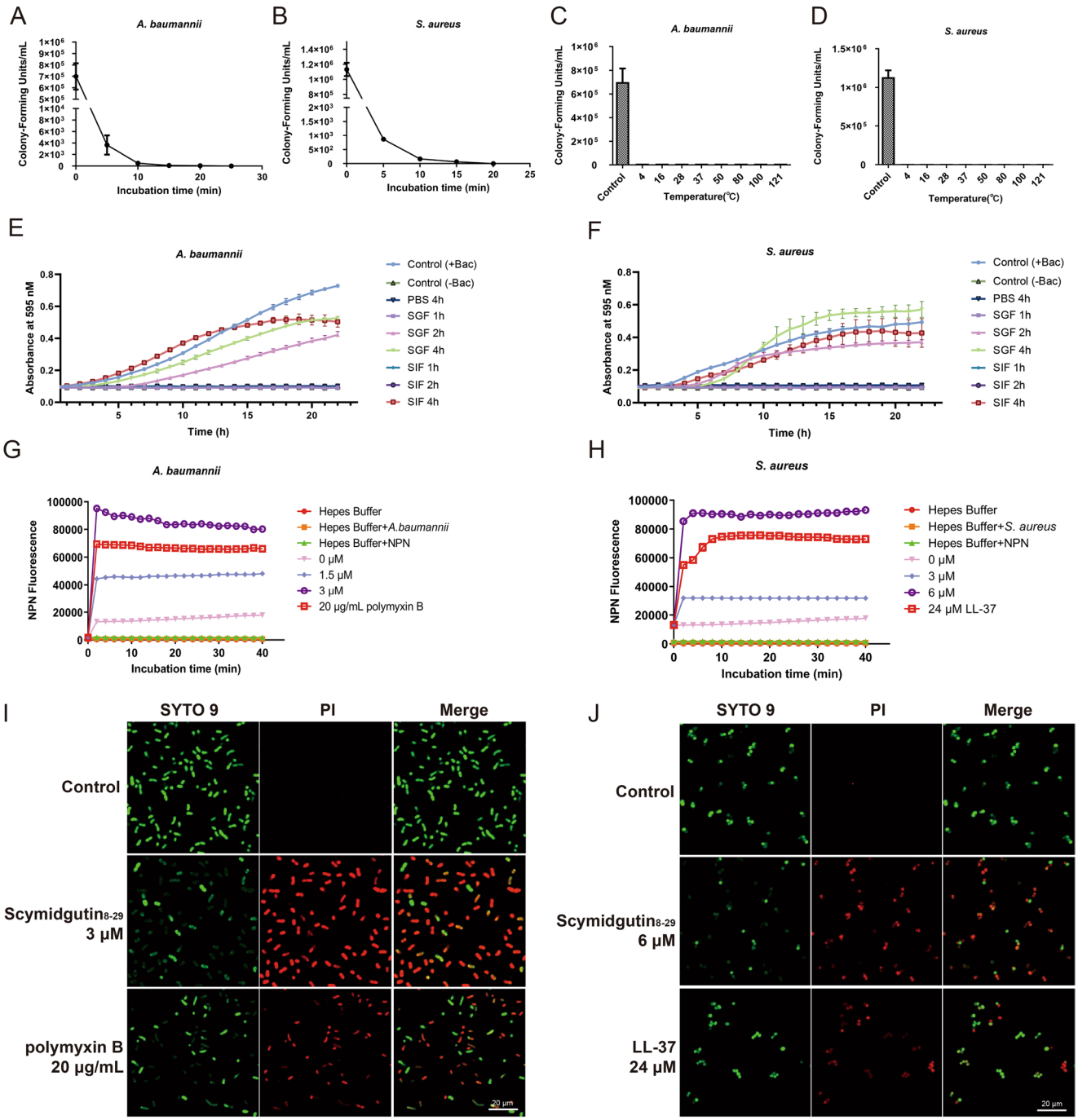



**Fig. 2** Antimicrobial properties and membrane disruption mechanism of Scymidgutin$_{8–29}$. (**A**, **B**) Time-kill kinetics against *A. baumannii* and *S. aureus* at 1×MIC. (**C**-**D**) Thermal stability was assessed by treating bacteria with the peptide incubated at the indicated temperatures. (**E**, **F**) Stability of Scymidgutin$_{8–29}$ in simulated gastrointestinal fluids. Residual antibacterial activity against *A. baumannii* (**E**) and *S. aureus* (**F**) after incubation in simulated intestinal fluid (SIF, pH 6.8, containing trypsin) and simulated gastric fluid (SGF, pH 2.0, containing pepsin) at 37 °C for 0, 1, 2, and 4 h. (**G**, **H**) Membrane permeability changes measured by NPN uptake. (**I**, **J**) Membrane integrity visualized by CLSM with SYTO 9 (green, live) and PI (red, dead) staining in *A. baumannii* CGMCC 1.6769 (**I**) and *S. aureus* CGMCC 1.2465 (**J**) following treatment with Scymidgutin$_{8–29}$, with LL-37 and PMB as positive controls

(predominantly neutrophils) compared to DSS controls (Fig. 7G). Concordantly, cytokine profiling demonstrated potent suppression of pro-inflammatory mediators (IL-1β, TNF-α, IL-6) and elevation of anti-inflammatory IL-10 in Scymidgutin$_{8–29}$-treated mice relative to DSS-challenged animals (Fig. 7H-K).

The gut microbiota, a key regulator in intestinal inflammation, was investigated for its role in Scymidgutin$_{8–29}$-mediated

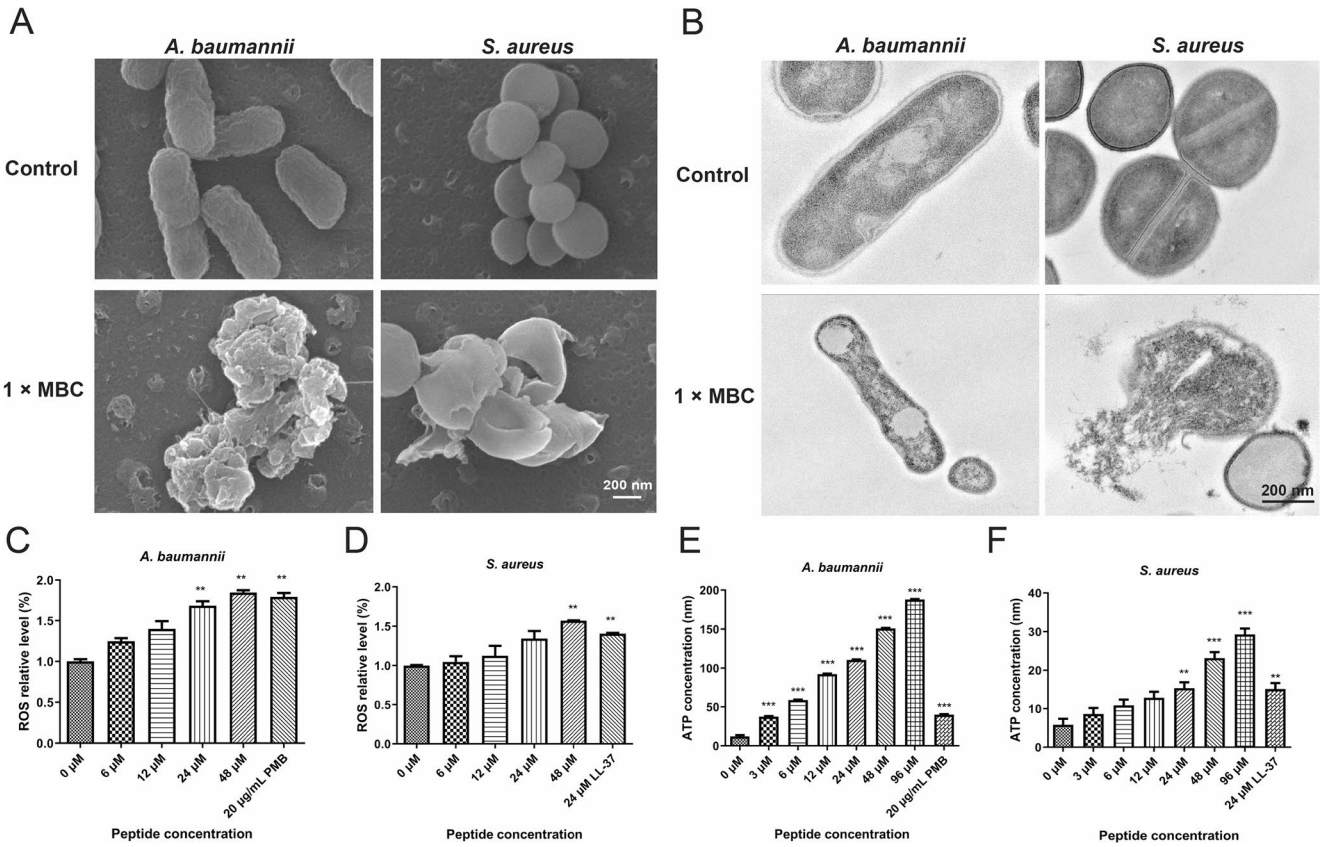



**Fig. 3** Mechanism of action of Scymidgutin$_{8–29}$. (**A**, **B**) SEM and TEM images showing morphological changes in *A. baumannii* and *S. aureus* after peptide treatment. (**C**, **D**) Measurement of intracellular ROS in *A. baumannii* (**C**) and *S. aureus* (**D**) following treatment with Scymidgutin$_{8–29}$. PMB (20 μg/mL) and LL-37 (24 μM) were used as positive controls for *A. baumannii* and *S. aureus*, respectively. (**E**, **F**) Promotion of intracellular ATP release. Data are mean ± SEM ($n = 3$). *$P < 0.05$, **$P < 0.01$, ***$P < 0.001$

improvement of IBD. 16 S rRNA sequencing revealed that Scymidgutin$_{8–29}$ administration significantly restructured microbial community composition in DSS-challenged mice (Fig. 8A). Alpha diversity analysis revealed that DSS treatment significantly reduced microbial richness (Chao1, $p < 0.001$) and diversity (Shannon, $p < 0.001$) compared with the normal control group. Treatment with Scymidgutin$_{8–29}$ significantly restored both indices relative to the DSS group (Chao1, $p < 0.01$; Shannon, $p < 0.001$) (Fig. 8B, C). Principal coordinate analysis (PCoA) based on weighted UniFrac distance revealed a clear separation of the DSS group from the other three groups, with the first two principal coordinates explaining 27.31% and 21.08% of the total variance, respectively. Notably, the Scymidgutin$_{8–29}$ group clustered in close proximity to the normal control group in the PCoA ordination space, indicating that Scymidgutin$_{8–29}$ treatment largely restored the microbial community structure toward a healthy composition (Fig. 8D). Microbiota profiling revealed that Scymidgutin$_{8–29}$ treatment significantly reduced the relative abundance of *Proteobacteria* and *Verrucomicrobiota* at the phylum level, with lower relative abundance of *Clostridia*, *Verrucomicrobiae*, and *Gammaproteobacteria* at the class level (Fig. 8E, F). Notably, a consistent lower relative abundance was observed along the Verrucomicrobiota lineage from phylum to genus *Akkermansia* in Scymidgutin$_{8–29}$-treated mice versus DSS controls (Fig. S4A–D). To further identify taxa most strongly associated with treatment, we performed LEfSe analysis. This identified *Rikenellaceae* as the taxon most strongly enriched in the Scymidgutin$_{8–29}$-treated group (Fig. S4E, F). These findings suggest that microbiota modulation is associated with the therapeutic activity of Scymidgutin$_{8–29}$.

## Discussion

The complex pathogenesis of IBD, driven by both intestinal microbiota dysbiosis and host immune dysregulation, is inadequately addressed by current single-target therapies, underscoring the need for agents with combined antimicrobial and immunomodulatory activities [37]. AMPs represent promising candidates in this regard, owing to their evolutionarily conserved dual functionality and adaptability to the intestinal microenvironment [38]. Marine crustacean AMPs,

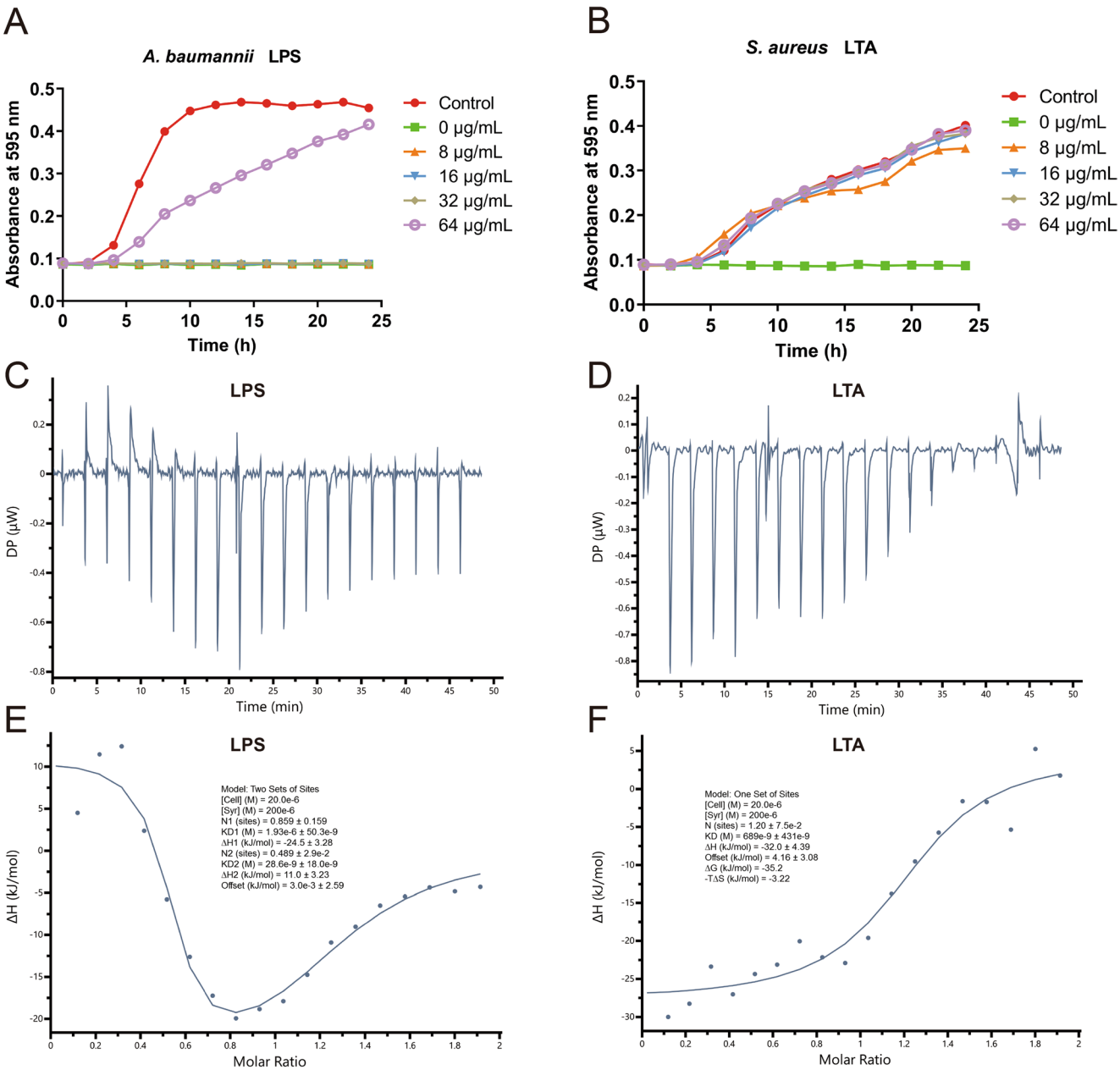



**Fig. 4** Competitive inhibition of Scymidgutin$_{8\text{-}29}$ antibacterial activity by LPS and LTA, and direct binding analysis by ITC. (**A**, **B**) Competitive inhibition assays: the antibacterial activity of Scymidgutin$_{8\text{-}29}$ (at a fixed concentration) against indicator bacteria was measured in the presence of increasing concentrations of exogenous LPS (**A**) or LTA (**B**). (**C**, **D**) ITC titration curves (differential power, DP) showing the raw heat signals per injection upon titrating 200 μM peptide into 20 μM LPS (**C**) or LTA (**D**) at 25 °C. (**E**, **F**) Integrated binding isotherms (enthalpy change per mole of injectant, ΔH) plotted against the molar ratio of peptide to LPS (**E**) or LTA (**F**). The LPS data were fitted to a two-site binding model (solid line in **E**) due to the biphasic heat profile, yielding: Site 1: $Kd_1$ = 1.93 μM, $N_1$ = 0.86, $\Delta H_1$ = -24.5 kJ/mol; Site 2: $Kd_2$ = 28.6 nM, $N_2$ = 0.49, $\Delta H_2$ = +11.0 kJ/mol. The LTA data were fitted to a one-site binding model (solid line in F), giving Kd = 689 nM, N = 1.20, ΔH = –32.0 kJ/mol, ΔG = -35.2 kJ/mol, -TΔS = -3.22 kJ/mol. All interactions are thermodynamically spontaneous (ΔG < 0)

in particular, have been widely studied for their broad-spectrum antimicrobial activity and immunoregulatory potential [30, 39]. However, their potential in mammalian models of intestinal inflammation remains largely unexplored. In this study, we identified Scymidgutin$_{8\text{–}29}$, a 22-residue cationic peptide from the mud crab *S. paramamosain*, and evaluated its antibacterial mechanism, immunomodulatory capacity, and in vivo efficacy in a DSS-induced colitis model. Scymidgutin$_{8\text{–}29}$ exhibited rapid membrane-disruptive bactericidal activity against MDR pathogens, promoted M2 macrophage

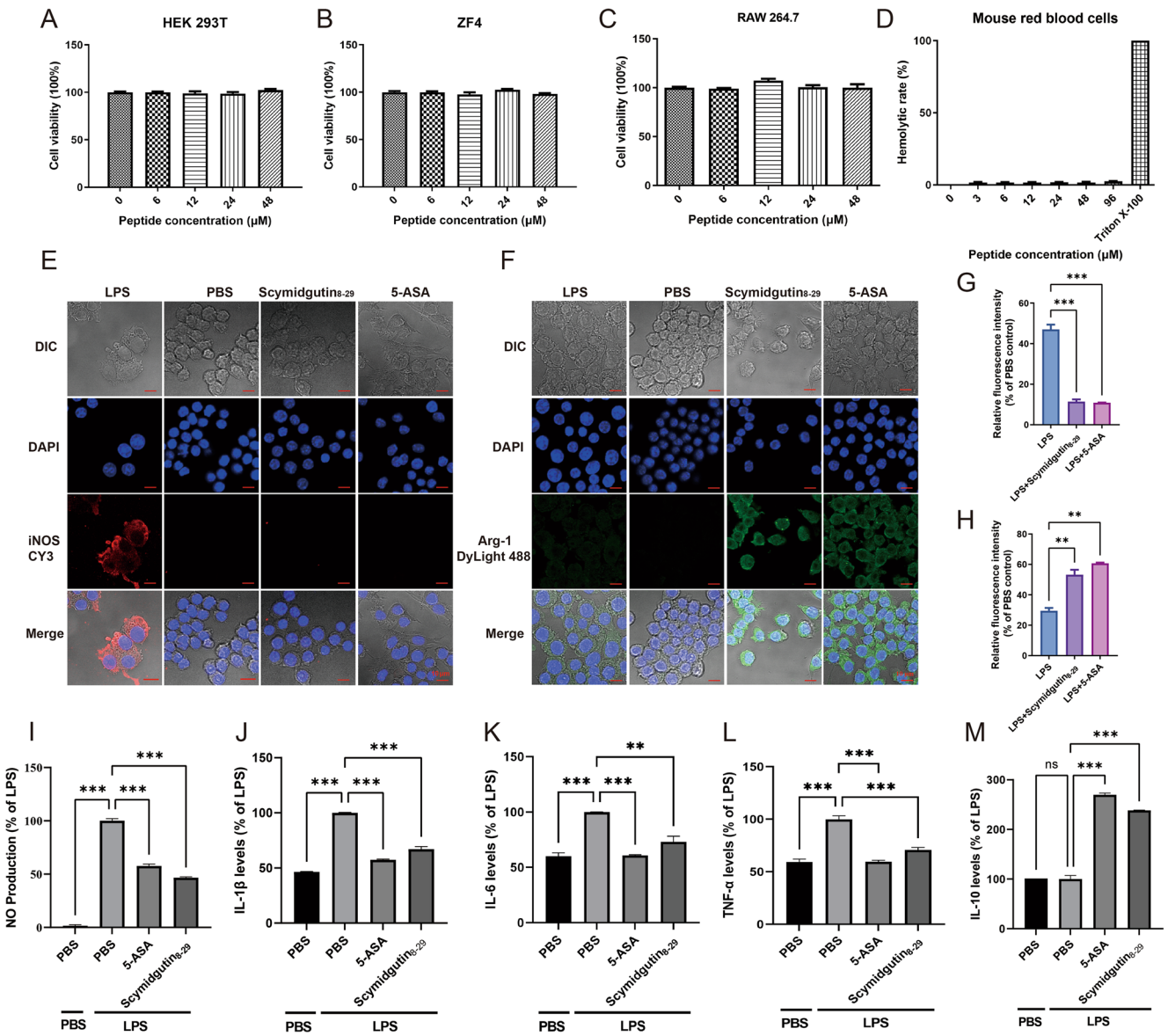



**Fig. 5** Evaluation of Scymidgutin$_{8–29}$'s biosafety and anti-inflammatory activity in vitro. (**A**-**C**) Cytotoxicity of Scymidgutin$_{8–29}$ at indicated concentrations was assessed in HEK-293T (**A**), ZF4 (**B**), and RAW 264.7 (**C**) cells using MTS assay. (**D**) Hemolytic activity against mouse erythrocytes. (**E**, **F**) Representative immunofluorescence staining of iNOS (**E**) and Arg-1 (**F**) in RAW264.7 macrophages with or without LPS induction and peptide treatment. (**G**, **H**) Quantification of mean fluorescence intensity of iNOS (**G**) and Arg-1 (**H**) staining. (**I**) Nitric oxide (NO) levels in the supernatant. (**J**-**M**) Cytokine levels (IL-1β, IL-6, TNF-α, IL-10) were measured by ELISA. Data are mean ± SEM ($n = 5$ independent experiments). *$P < 0.05$, **$P < 0.01$, ***$P < 0.001$, vs. indicated groups by two-tailed Student's t-test or one-way ANOVA

polarization, and significantly ameliorated DSS-induced colitis with altered gut microbiota composition. These findings position Scymidgutin$_{8–29}$ as a promising multi-functional candidate for intestinal inflammation and expand the therapeutic potential of crustacean-derived AMPs.

We first characterized the antimicrobial activity of Scymidgutin$_{8–29}$ in vitro. The peptide exhibited broad-spectrum antibacterial activity at low micromolar concentrations against both Gram-negative and Gram-positive pathogens, including multidrug-resistant clinical isolates such as MRSA and MDR *A. baumannii*. It also effectively inhibited key intestinal pathogenic and commensal bacteria. Mechanistic studies indicated that Scymidgutin$_{8–29}$ exerts its bactericidal effect primarily through rapid and irreversible membrane disruption. Ultrastructural analysis by SEM and TEM revealed extensive membrane damage and cytoplasmic leakage in both species, consistent with NPN uptake and SYTO9/PI staining, which confirmed outer membrane permeabilization in *A. baumannii* and cytoplasmic membrane perturbation in *S. aureus*. This membrane-targeting

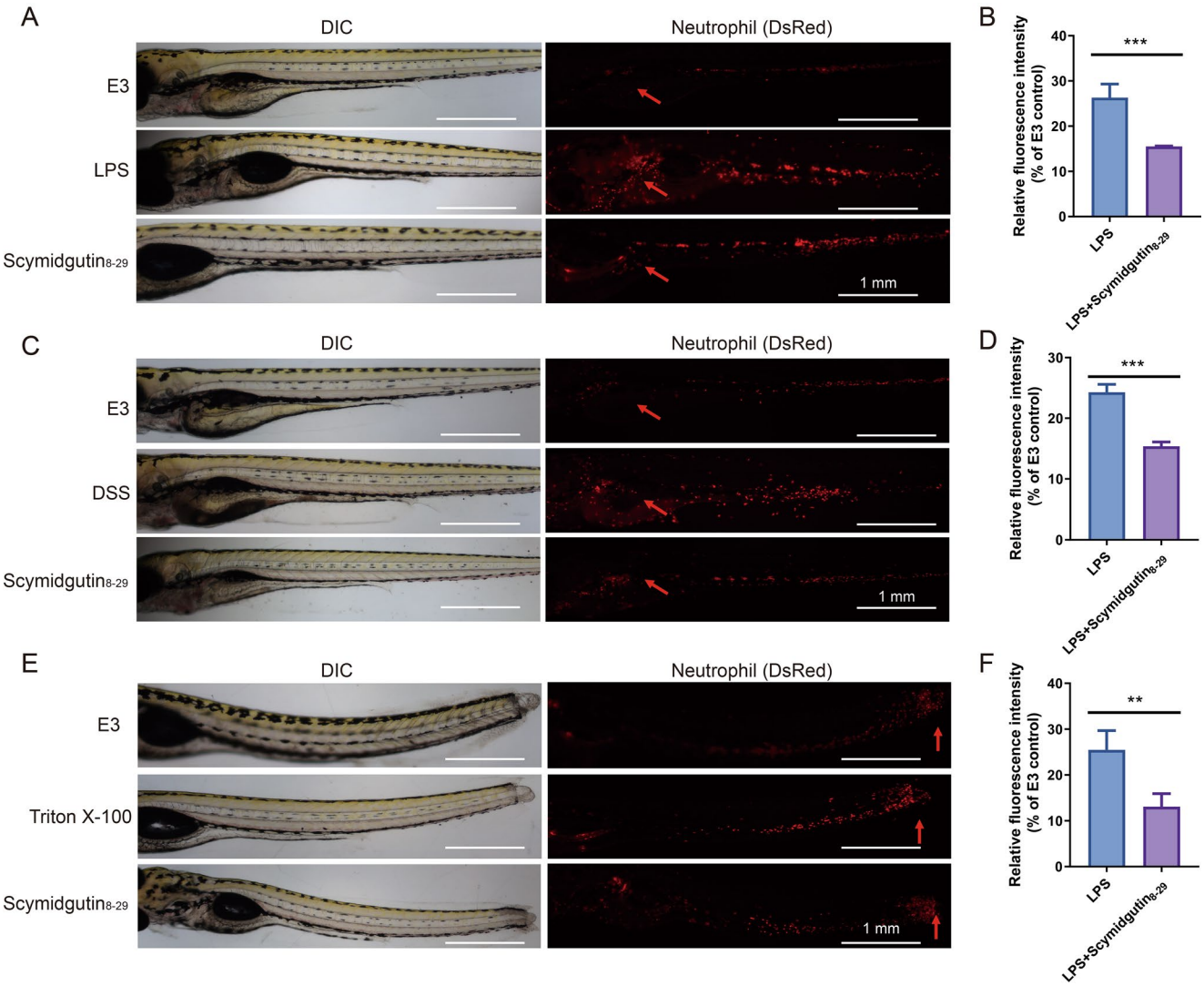



**Fig. 6** Scymidgutin$_{8–29}$ inhibits neutrophil recruitment in a transgenic zebrafish inflammation model. Tg(lyz: DsRed) zebrafish were subjected to LPS treatment, DSS exposure, or tail fin amputation. Representative whole-body fluorescent images show neutrophil distribution (red) in (**A**) LPS-treated, (**C**) DSS-treated, and (**E**) tail-injured zebrafish following treatment with Scymidgutin$_{8–29}$ or vehicle control. Quantification of mean fluorescence intensity in the hindbrain region in (**B**) LPS and (**D**) DSS models, and (**F**) at the wound site in the tail fin amputation model. Data are mean ± SEM ($n = 20$ larvae per group). *$P < 0.05$, **$P < 0.01$, ***$P < 0.001$ vs. indicated groups by one-way ANOVA with Tukey's post-hoc test

mechanism underlies the peptide's rapid bactericidal kinetics (> 99.9% reduction within 20 min at 1×MBC), a feature considered advantageous for reducing the likelihood of resistance development compared with conventional antibiotics, although dedicated resistance induction studies are required to confirm this assumption [40]. The successful design of Scymidgutin$_{8–29}$ from the full-length 67-amino-acid protein can be attributed to the structural features of the 8–29 region. As predicted by helical wheel projection, this segment contains a high proportion of positively charged residues (arginine and lysine) and hydrophobic residues arranged in a spatially segregated amphipathic distribution, which is a hallmark of membrane-active AMPs.

The ITC data not only confirm direct binding of Scymidgutin$_{8–29}$ to both LPS and LTA but also reveal distinct thermodynamic mechanisms. The biphasic (V-shaped) isotherm for LPS, with an initial exothermic phase followed by an endothermic phase, is consistent with a two-step binding process: an initial electrostatic recognition (Site 1, $\Delta H < 0$) and a subsequent entropy-driven insertion that disrupts LPS supramolecular aggregates (Site 2, $\Delta H > 0$). This is in line with the known ability of cationic amphipathic peptides to destabilize LPS micelles. In contrast, the single-site exothermic binding to LTA suggests a more homogeneous interaction, predominantly electrostatic in nature. These complementary binding modes support the

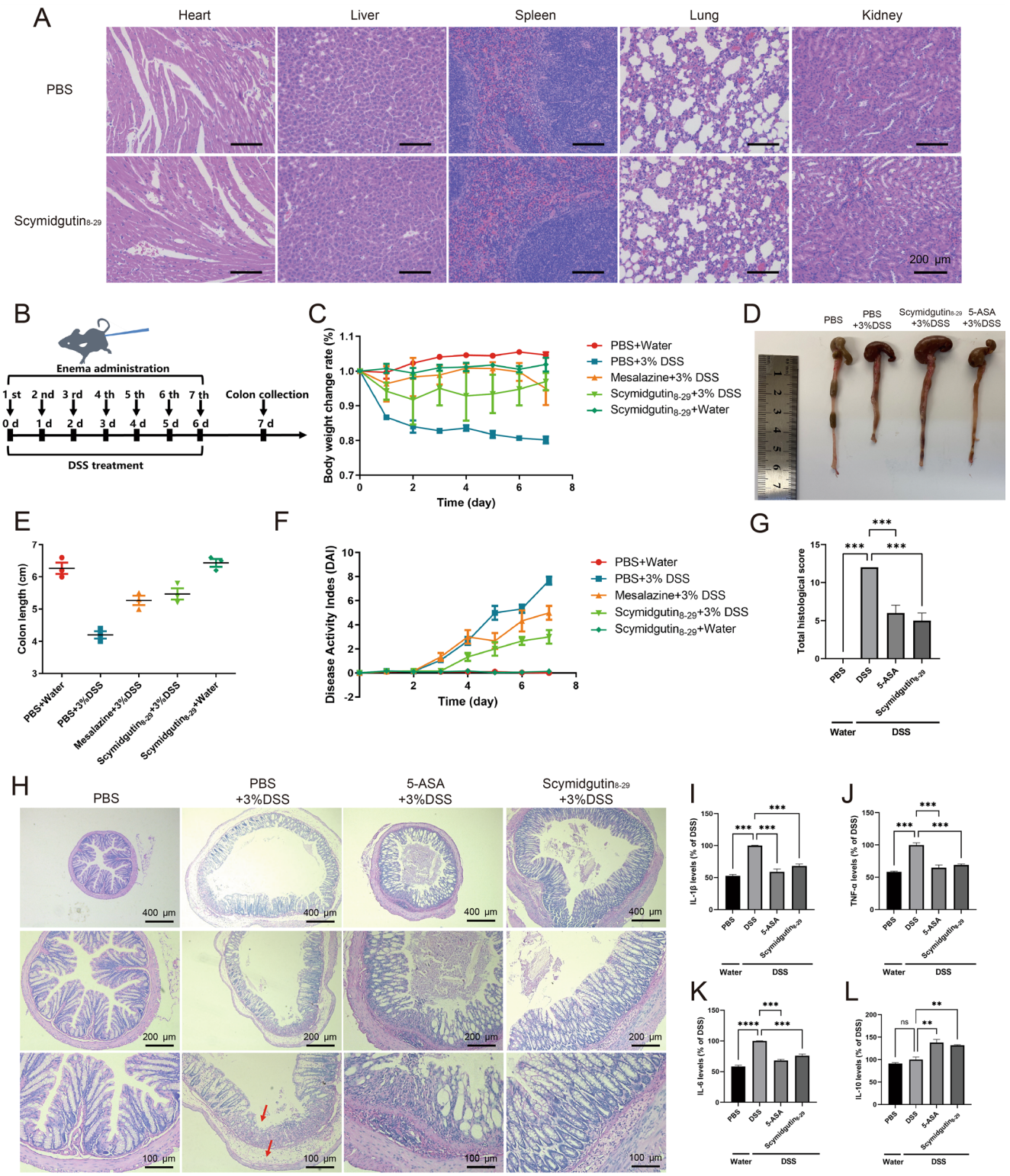



**Fig. 7** Scymidgutin$_{8–29}$ ameliorates DSS-induced colitis in mice. (**A**) Representative images of visceral tissues show no overt toxicity. (**B**) Experimental timeline. C57BL/6 mice received 3% DSS in drinking water from day 0 to 7, concurrently with daily intrarectal administration of PBS, Scymidgutin$_{8–29}$, or Mesalazine. (**C**) Body weight changes. (**D**) Representative colon photographs and (**E**) their quantified lengths on day 7. (**F**) Disease Activity Index (DAI) score. (**G**) Total histological score (range, 0–12) calculated as the sum of epithelial damage, inflammatory infiltration, and crypt destruction scores (each scored 0–4). (**H**) Representative H&E-stained colon sections. (**I-L**) Cytokine levels in colon tissues were measured by ELISA on day 7. Data are mean ± SEM ($n = 10$ mice per group). *$P < 0.05$, **$P < 0.01$, ***$P < 0.001$, vs. DSS group by two-tailed Student's t-test or one-way ANOVA

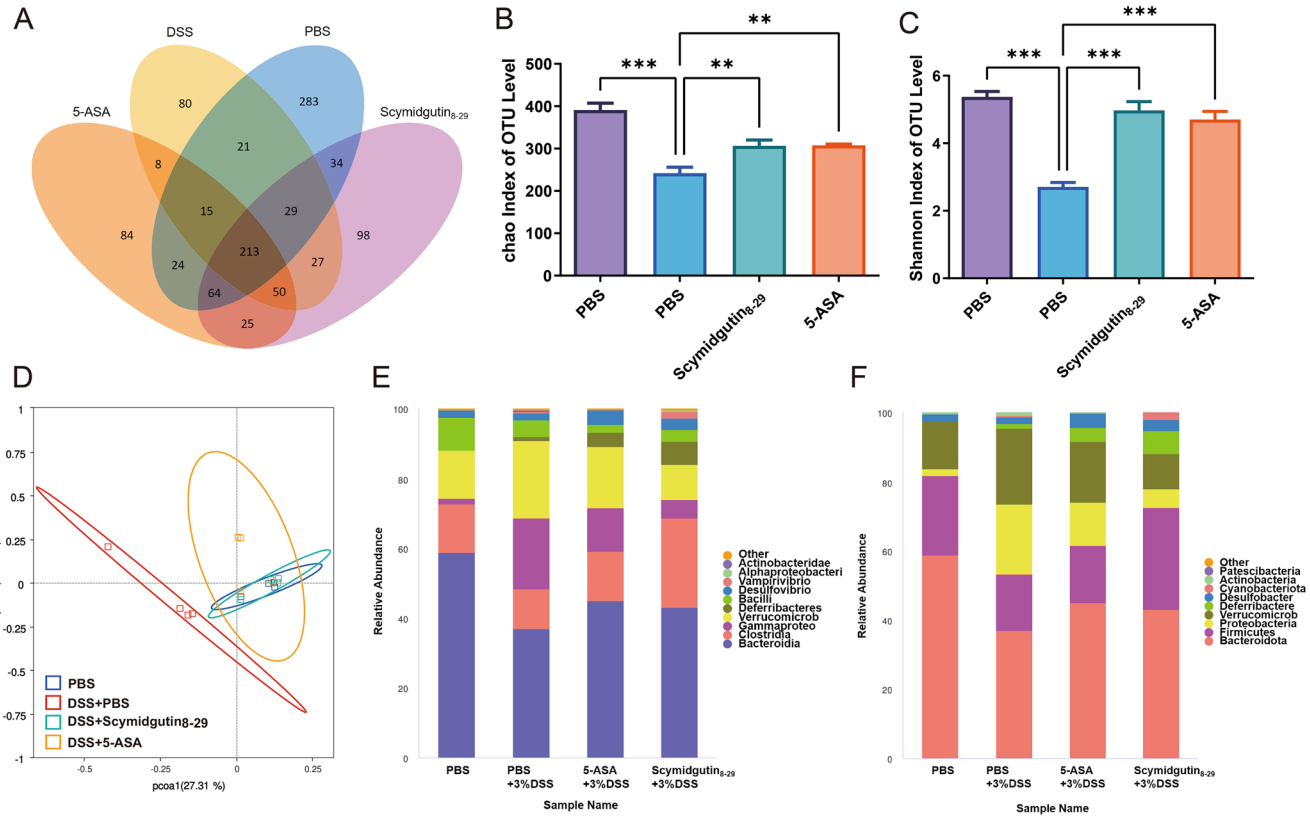



**Fig. 8** Scymidgutin$_{8–29}$ alters the gut microbiota composition in DSS-induced colitis mice. Fecal samples were collected on day 7 and analyzed by 16 S rRNA gene sequencing ($n = 10$ per group). (**A**) Flower diagram showing the number of shared and unique ASVs among the four groups. Each petal represents a group, and the center indicates the number of ASVs shared by all groups. (**B**, **C**) Alpha diversity indices: (**B**) Chao1 richness estimator and (**C**) Shannon diversity index. Data are presented as box plots (median, interquartile range, and min–max); *p* values were determined by Kruskal-Wallis test with Dunn's post-hoc test for pairwise comparisons. $^{*}P<0.05$, $^{**}P<0.01$ vs. indicated groups. (**D**) Principal coordinate analysis (PCoA) based on weighted UniFrac distance. Each point represents one fecal sample; ellipses represent 95% confidence intervals. The first two principal coordinates explained 27.31% (PCoA1) and 21.08% (PCoA2) of the total variance. (**E**, **F**) Relative microbial abundance at the phylum and class levels

peptide's broad-spectrum membrane-disrupting activity against both Gram-negative and Gram-positive bacteria, and provide a structural rationale for its potent antibacterial effects observed in the present study.The antimicrobial properties of Scymidgutin$_{8–29}$ compare favorably with those of several well-characterized AMPs. The human cathelicidin LL-37 exhibits broad-spectrum antibacterial activity but is susceptible to proteolytic degradation, which may limit its application in the intestine [41–43]. Similarly, marine-derived AMPs such as ALFs and crustins possess potent in vitro antibacterial activity but have rarely been evaluated in mammalian colitis models [32, 33]. In comparison, Scymidgutin$_{8–29}$ achieves more rapid bactericidal kinetics (> 99.9% killing within 20 min) and retains potent activity against MDR clinical isolates (MIC 1.5–24 μM).

Recent advances in peptide-based therapeutics further support the translational potential of our findings. Peptides such as OA-AL14 and OL-RA11, as well as other bioactive peptides, have demonstrated efficacy in modulating inflammation and preserving barrier integrity [24–29]. Scymidgutin$_{8–29}$ adds to this growing body of evidence by combining membrane-disrupting antibacterial activity with macrophage repolarization, a dual mechanism that is particularly relevant to IBD, where both microbial dysbiosis and immune dysregulation contribute to pathogenesis.

Beyond its direct antibacterial activity, Scymidgutin$_{8–29}$ displayed significant anti-inflammatory properties. The peptide showed no cytotoxicity in normal mammalian (HEK-293T, RAW 264.7) and zebrafish (ZF4) cell lines, and the absence of hemolytic activity highlights its favorable biocompatibility. Crucially, Scymidgutin$_{8–29}$ exhibited profound immunomodulatory effects in vitro, shifting LPS-stimulated macrophages from a pro-inflammatory M1 state (characterized by elevated iNOS, NO, IL-6, TNF-α, and IL-1β) toward an anti-inflammatory M2 state (increased Arg-1 and IL-10). Macrophage polarization is a central regulator of inflammation resolution and tissue repair [44, 45], and modulating this axis represents a promising

therapeutic strategy for inflammatory diseases [45]. The significant suppression of pro-inflammatory cytokines and elevation of IL-10 by Scymidgutin$_{8–29}$ confirms its potent anti-inflammatory capacity in vitro. The absence of cytotoxicity and hemolytic activity, despite potent membrane-disrupting activity against bacteria, reflects the selective targeting of bacterial over mammalian membranes. This selectivity is largely attributable to differences in membrane lipid composition: bacterial membranes are rich in negatively charged phospholipids (e.g., phosphatidylglycerol and cardiolipin) and contain LPS or LTA, which promote electrostatic interactions with the cationic peptide [46]. In contrast, mammalian plasma membranes are consist predominantly of zwitterionic phospholipids (phosphatidylcholine and sphingomyelin) which exhibit lower affinity for cationic peptides. Furthermore, cholesterol in mammalian membranes may stabilize the bilayer and impede peptide insertion, collectively contributing to the favorable selectivity of Scymidgutin$_{8–29}$.

In three complementary zebrafish larva models, Scymidgutin$_{8–29}$ consistently inhibited inflammation-driven neutrophil trafficking in vivo. The attenuation of neutrophil migration to sites of chemical inflammation (LPS/DSS) and physical injury (caudal fin transection) indicates that Scymidgutin$_{8–29}$ can interfere with key chemotactic pathways in vivo. In the DSS-induced acute colitis model, Scymidgutin$_{8–29}$ effectively ameliorated hallmark features of DSS-induced colitis, a widely used model of acute intestinal inflammation. The peptide significantly mitigated weight loss, reduced the DAI score, prevented colon shortening, and restored colonic epithelial architecture while diminishing neutrophil-rich inflammatory infiltrate. This histopathological improvement was accompanied by a shift in the colonic cytokine milieu: Scymidgutin$_{8–29}$ treatment significantly suppressed pro-inflammatory mediators (IL-1β, TNF-α, IL-6) while elevating anti-inflammatory IL-10 [47, 48]. This cytokine modulation is consistent with the peptide's in vitro capacity to repolarize macrophage, suggesting that Scymidgutin$_{8–29}$ may promote an anti-inflammatory microenvironment in the inflamed gut.

The immunomodulatory profile of Scymidgutin$_{8–29}$ also compares favorably with existing AMPs. Its ability to promote M2 macrophage polarization is not commonly reported among crustacean AMPs. Together with its exceptional thermostability (retaining activity across 4–121 °C) and demonstrated in vivo efficacy in a murine colitis model, Scymidgutin$_{8–29}$ represents a distinctive candidate within the expanding landscape of marine-derived immunomodulatory AMPs.

Dysbiosis, characterized by reduced microbial diversity and expansion of specific pro-inflammatory taxa, is a hallmark of IBD and actively contributes to pathogenesis [49, 50]. However, the causal relationship between dysbiosis and intestinal inflammation remains controversial; while some studies propose dysbiosis as a primary driver of pathogenesis, others view it as a secondary consequence of the inflammatory environment [51]. Our current data do not allow us to differentiate between these possibilities. Notably, the microbiota alterations observed following Scymidgutin$_{8-29}$ treatment could arise from direct antimicrobial actions, indirect effects secondary to amelioration of inflammation, or a combination of both, thus necessitating further mechanistic studies, for instance, using germ-free or antibiotic-depleted models, to clarify their relative contributions. Regardless of whether dysbiosis is a cause or consequence of inflammation, Scymidgutin$_{8–29}$ may break this vicious cycle via its dual actions: direct antibacterial effects against pathobionts and anti-inflammatory activity via M2 macrophage polarization. Thus, even if dysbiosis is secondary to mucosal defects [51], Scymidgutin$_{8–29}$ could still benefit IBD by acting on both microbial and host inflammatory components.

In this regard, AMP fragments represent a particularly relevant class of molecules, as they are capable of directly interacting with the microbial community while concurrently modulating host inflammatory responses. Studies have demonstrated that mammalian defensin-derived peptides, including human defensin-5, porcine β-defensin 2, and their fragments, exert protective effects in DSS-induced colitis and other intestinal injury models, primarily through the regulation of tight junction proteins (e.g., ZO-1, occludin) and mucin expression, thereby enhancing epithelial barrier integrity [52–54]. Recently, Rosa et al. further showed that orally administered human defensin fragments HD5$_{1-9}$ and hBD2 improved gut barrier function and metabolic parameters in mice fed a Western-style diet [55]. These findings support the therapeutic potential of AMP fragments in intestinal disorders. Our study extends this paradigm by demonstrating that a crustacean-derived peptide, Scymidgutin$_{8–29}$, with a distinct membrane-disrupting mechanism, is similarly effective in the DSS-induced colitis model, offering a complementary mechanistic approach to mammalian defensin fragments.

The microbial changes observed after Scymidgutin$_{8–29}$ treatment should be interpreted with caution. LEfSe analysis identified *Rikenellaceae* as the taxon most strongly enriched in the Scymidgutin$_{8–29}$-treated group. Members of *Rikenellaceae* have been reported to be negatively associated with pro-inflammatory cytokine levels and to decrease remarkably in DSS-treated colitis mice [56], suggesting that this enrichment may represent a beneficial microbial shift. However, 16 S rRNA V4 sequencing does not provide species-level resolution. The genus *Akkermansia* contains multiple species with distinct and sometimes opposing functions. Although *A. muciniphila* is generally considered beneficial

in metabolic contexts, recent evidence indicates that its role in intestinal inflammation is context-dependent, with both protective and pro-inflammatory effects reported depending on the model and inflammatory milieu [57–59]. In addition, Proteobacteria and Verrucomicrobiota are broad taxa comprising heterogeneous members; therefore, changes in their relative abundance should not be interpreted as specific loss or gain of pathogenic or beneficial species. Moreover, the reduction in *Akkermansia* and *Proteobacteria* could result from either a direct antimicrobial effect of Scymidgutin$_{8–29}$ or a secondary consequence of inflammation resolution. Thus, the causal relationship between these microbial shifts and colitis amelioration remains to be established. Future studies using species-level metagenomics, culturomics, or targeted quantification will be needed to determine which taxa mediate the protective effects.

The observation that Scymidgutin$_{8–29}$ treatment restored microbial diversity and reduced pro-inflammatory taxa could reflect either a direct antimicrobial effect of the peptide on the gut microbiota or an indirect consequence of inflammation resolution, or a combination of both. In this regard, it is important to note that inflammation itself profoundly alters gut microbial composition [60]. Notably, 5-ASA also induced microbial changes in our study, suggesting that a considerable proportion of the microbiota modulation observed with Scymidgutin$_{8–29}$ treatment may be secondary to the resolution of intestinal inflammation, rather than exclusively a direct consequence of its antibacterial action. This interpretation is consistent with the concept that the inflammatory milieu, rather than the presence or absence of specific taxa per se, drives dysbiosis in colitis [51]. Nevertheless, the direct membrane-disrupting activity of Scymidgutin$_{8–29}$ against intestinal pathobionts in vitro raises the possibility that both direct and indirect mechanisms contribute to the observed microbiota alterations in vivo.

Notably, the present data do not establish whether the observed in vivo protection depends on the peptide's direct antibacterial activity, its immunomodulatory properties, or both. DSS-induced colitis is a chemical injury model driven primarily by epithelial barrier disruption and innate inflammatory responses [61, 62]; thus, the therapeutic benefit of Scymidgutin$_{8–29}$ could be attributable to its direct anti-inflammatory effects, including the promotion of M2 macrophage polarization and suppression of pro-inflammatory cytokines, which could create a mucosal environment conducive to inflammation resolution [63]. The reductions in the relative abundance of pro-inflammatory taxa such as *Proteobacteria* and *Akkermansia* may represent a secondary consequence of restored mucosal homeostasis rather than a direct effect of bacterial killing [49]. Alternatively, direct bactericidal activity against specific pathobionts might contribute indirectly to immune regulation by reducing luminal inflammatory stimuli, although this remains speculative. Further studies using germ-free mice, microbiota depletion models, or macrophage-specific knockout systems are warranted to determine whether the antimicrobial and immunomodulatory functions contribute independently, sequentially, or redundantly to the observed therapeutic effects [64, 65]. The broad-spectrum membrane-disrupting activity of Scymidgutin$_{8–29}$, together with its association with a shift in gut microbial community composition toward a less inflammatory profile, suggests that its antimicrobial and immunomodulatory properties may act in concert to break the dysbiosis-inflammation cycle that characterizes intestinal inflammation.

Beyond its direct antibacterial and immunomodulatory activities, Scymidgutin$_{8–29}$ may act through a third, conceptually distinct mechanism involving interaction with the colonic mucus layer. Accumulating evidence identifies microbial attachment to and invasion of the intestinal mucosa as a fundamental defect in IBD pathogenesis, with chronic inflammation persisting as long as the mucus barrier remains defective [66, 67]. Given its cationic and membrane-active properties, Scymidgutin$_{8–29}$ could plausibly integrate into the the negatively charged mucin network, thereby reinforcing the physical barrier and limiting bacterial encroachment toward the epithelial surface. Although the present study did not directly assess mucus-associated bacterial density, mucus thickness, or local defensin expression, these parameters represent critical endpoints for future mechanistic investigations.

Resistance development against Scymidgutin$_{8–29}$ is a relevant consideration. Membrane-disrupting AMPs are generally less prone to resistance than conventional antibiotics, although membrane modification, proteolytic degradation, and efflux-based resistance have been reported for other AMPs [40, 68]. The rapid bactericidal kinetics of Scymidgutin$_{8–29}$ may limit the window for resistance emergence, and combination therapy or structural optimization could further reduce this risk.

The potential immunogenicity of Scymidgutin$_{8–29}$ upon repeated administration also warrants consideration. Published evidence on the immunogenicity of AMPs after repeated dosing remains limited. Plectasin, a 4.4 kDa antimicrobial peptide, elicited no antibody response in mice treated for 5 days with one to two daily subcutaneous doses, but low levels of antibodies developed in approximately half of the animals after a subsequent immunization following a rest period [69]. This finding suggests that repeated exposure may pose a risk of antibody development in certain individuals, although the impact on therapeutic efficacy remains unclear. The relationship between peptide length and immunogenicity is also relevant. $CD4^+$ T lymphocytes

usually recognize peptides of 12–16 amino acids in the context of HLA class II molecules, but pentapeptides, tetrapeptides, and even tripeptides can be recognized by T cell clones in certain contexts [70]. Although short peptides are generally considered to have intrinsic low immunogenicity [71], a definitive conclusion that short peptides are non-immunogenic has not been established. For Scymidgutin$_{8–29}$ (22 residues), the short linear structure and intrarectal delivery may limit systemic exposure and antibody development; nevertheless, dedicated immunogenicity assessment, including measurement of anti-peptide IgG after repeated dosing, will be necessary to evaluate its long-term efficacy and safety.

Translational development of peptide-based IBD therapeutics faces several challenges, including manufacturing cost, stability, delivery, and regulatory requirements [72, 73]. Proteolytic instability remains a major obstacle to oral delivery. Although Scymidgutin$_{8–29}$ showed acceptable stability in simulated gastrointestinal fluids, its susceptibility to proteases limits oral delivery, and formulation strategies such as encapsulation, nanocarriers, hydrogels, suppositories, or enema-based local delivery, as well as protease-resistant analogs, will be needed to broaden its clinical applicability. Regulatory pathways for peptide therapeutics typically require comprehensive preclinical safety assessment, pharmacokinetic and pharmacodynamic characterization, immunogenicity evaluation, and phase-appropriate GMP manufacturing before clinical trials. Thus, while Scymidgutin$_{8–29}$ shows promising activity, substantial optimization and formal preclinical development will be required before clinical translation can be considered. The present study has several limitations that should be acknowledged. First, the therapeutic efficacy of Scymidgutin$_{8–29}$ was evaluated in a DSS-induced acute colitis model. Although this model is widely used and recapitulates key features of epithelial barrier disruption and innate

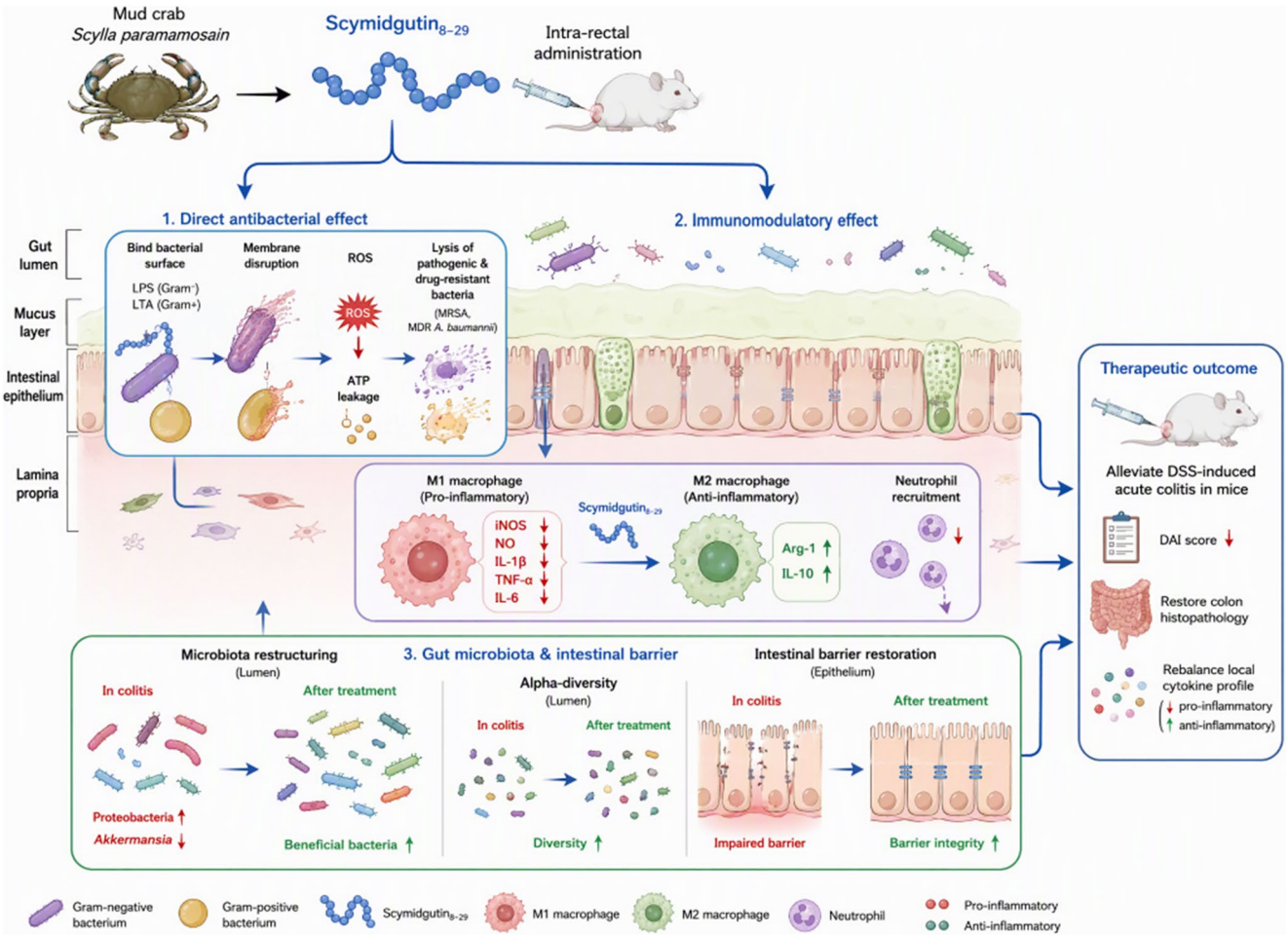



**Fig. 9** Schematic illustration of the proposed dual mechanism of action of Scymidgutin$_{8–29}$ in DSS-induced colitis. Scymidgutin$_{8–29}$ exerts direct antibacterial activity by binding to bacterial surface components (LPS and LTA), disrupting membrane integrity, and causing rapid bacterial death. In parallel, the peptide modulates host immunity by promoting M2 macrophage polarization and suppressing pro-inflammatory cytokines (IL-1β, TNF-α, IL-6), while elevating IL-10. In DSS-induced colitis, these dual actions contribute to reduced disease severity, restored colonic histopathology, and remodeling of the gut microbiota

immune activation, it is a chemically induced injury model and does not fully recapitulate the chronic, relapsing-remitting course of human IBD [61, 62]. It also does not reproduce the complex genetic susceptibility andadaptive immune components of the disease. Therefore, the present results should be regarded as preclinical proof of concept rather than direct evidence of clinical efficacy. Validation in chronic colitis models, such as IL-10$^{-/-}$ mice or adoptive T cell transfer models, will be necessary before clinical translation. Second, although Scymidgutin$_{8–29}$ exhibited appreciable tolerance to simulated gastrointestinal fluids, its enzymatic stability remains suboptimal for systemic or oral delivery. Future efforts aimed at enhancing protease resistance, such as D-amino acid substitution, cyclization, or formulation with protease inhibitors, will be essential to broaden its translational potential. Third, although Scymidgutin$_{8–29}$ exhibits both antibacterial and immunomodulatory activities, the present in vivo data do not establish whether its therapeutic efficacy is dependent primarily on antibacterial activity, immunomodulatory activity, or both. The observed reductions in bacterial burden and inflammatory responses are correlative, and the two activities may act independently, sequentially, or redundantly. Future studies using a non-bactericidal mutant of Scymidgutin$_{8–29}$, macrophage depletion with clodronate liposomes, macrophage-specific knockout mice, germ-free or microbiota-depleted models, and species-level microbial profiling (full-length 16 S sequencing or metagenomics) will be necessary to dissect these contributions and to establish causality. Until such experiments are performed, conclusions regarding the mechanism of action should be drawn with caution.

## Conclusion

In summary, this study identifies Scymidgutin$_{8–29}$ as a novel marine-derived cationic peptide from *S. paramamosain* that possesses both membrane-disruptive antibacterial activity and immunomodulatory properties (Fig. 9). In vitro, the peptide exhibited rapid, broad-spectrum bactericidal activity against clinically relevant pathogens, including multidrug-resistant strains, through a membrane-targeting mechanism, and promoted M2 macrophage polarization-while suppressing pro-inflammatory cytokine production. In a DSS-induced acute colitis mouse model, Scymidgutin$_{8–29}$ treatment significantly ameliorated disease severity, restored colonic histopathology, rebalanced cytokine profiles, and was associated with alterations in gut microbiota composition, notably a reduced relative abundance of colitis-associated *Akkermansia* and *Proteobacteria*. As summarized in Fig. 9, these dual antibacterial and immunomodulatory actions may act in concert to break the dysbiosis-inflammation cycle and promote intestinal barrier recovery. Although the relative contributions of its antimicrobial and immunomodulatory activities to the in vivo efficacy remain to be determined, these findings collectively position Scymidgutin$_{8–29}$ as a promising multi-functional candidate for further investigation in the context of intestinal inflammation.

**Supplementary Information** The online version contains supplementary material available at https://doi.org/10.1007/s12602-026-11247-9.

**Acknowledgements** We thank Mingyu Li (State Key Laboratory of Cellular Stress Biology, Xiamen University) for providing the Transgenic zebrafish. We thank Hui Peng, Huiyun Chen, Zhiyong Lin, Hua Hao, Ming Xiong and Xiao Hong (State Key Laboratory of Marine Environmental Science, Xiamen University) for technical assistance.

**Author Contributions** Chang Zhang: Data curation; Formal analysis; Investigation; Methodology; Writing-original draft. Xianxian Dong: Investigation and methodology. Ning Ding: Investigation and methodology. Fangyi Chen: Conceptualization; Funding acquisition; Project administration; Supervision; Writing-review and editing. Ke-Jian Wang: Conceptualization; Funding acquisition; Project administration; Supervision; Writing-review and editing.

**Funding** This work was supported by the National Natural Science Foundation of China with grant number (42376089); Fujian Ocean and Fisheries Bureau with grant number (FJHYF-L-2025-13); Fujian Province Industry-Academia Collaboration Project (2025N5001); Xiamen Ocean Development Bureau with grant number (22CZP002HJ08), and Pingtan Research Institute of Xiamen University with grant number (Z20220743).

**Data Availability** No datasets were generated or analysed during the current study.

## Declarations

**Competing interests** The authors declare no competing interests.

## References

1. Khor B, Gardet A, Xavier RJ (2011) Genetics and pathogenesis of inflammatory bowel disease. Nature 474:307–317. https://doi.org/10.1038/nature10209
2. de Souza HS, Fiocchi C (2016) Immunopathogenesis of IBD: current state of the art. Nat Rev Gastroenterol Hepatol 13:13–27. https://doi.org/10.1038/nrgastro.2015.186
3. Ruel J, Ruane D, Mehandru S et al (2014) IBD across the age spectrum: is it the same disease? Nat Rev Gastroenterol Hepatol 11:88–98. https://doi.org/10.1038/nrgastro.2013.240
4. Ni J, Wu GD, Albenberg L, Tomov VT (2017) Gut microbiota and IBD: causation or correlation? Nat Rev Gastroenterol Hepatol 14:573–584. https://doi.org/10.1038/nrgastro.2017.88
5. Courth LF, Ostaff MJ, Mailänder-Sánchez D et al (2015) Crohn's disease-derived monocytes fail to induce Paneth cell defensins. Proc Natl Acad Sci U S A 112:14000–14005. https://doi.org/10.1073/pnas.1510084112
6. Wehkamp J, Salzman NH, Porter E et al (2005) Reduced Paneth cell alpha-defensins in ileal Crohn's disease. Proc Natl

Acad Sci U S A 102:18129–18134. https://doi.org/10.1073/pnas.0505256102
7. Gersemann M, Wehkamp J, Fellermann K, Stange EF (2008) Crohn's disease—defect in innate defence. World J Gastroenterol 14:5499–5503. https://doi.org/10.3748/wjg.14.5499
8. Palmela C, Chevarin C, Xu Z et al (2018) Adherent-invasive *Escherichia coli* in inflammatory bowel disease. Gut 67:574–587. https://doi.org/10.1136/gutjnl-2017-314903
9. Martín R, Rios-Covian D, Huillet E et al (2023) *Faecalibacterium*: a bacterial genus with promising human health applications. FEMS Microbiol Rev 47:fuad039. https://doi.org/10.1093/femsre/fuad039
10. Quévrain E, Maubert MA, Michon C et al (2016) Identification of an anti-inflammatory protein from *Faecalibacterium prausnitzii*, a commensal bacterium deficient in Crohn's disease. Gut 65:415–425. https://doi.org/10.1136/gutjnl-2014-307649
11. Machiels K, Joossens M, Sabino J et al (2014) A decrease of the butyrate-producing species Roseburia hominis and *Faecalibacterium prausnitzii* defines dysbiosis in patients with ulcerative colitis. Gut 63:1275–1283. https://doi.org/10.1136/gutjnl-2013-304833
12. Papamichael K, Afif W, Drobne D et al (2022) Therapeutic drug monitoring of biologics in inflammatory bowel disease: unmet needs and future perspectives. Lancet Gastroenterol Hepatol 7:171–185. https://doi.org/10.1016/S2468-1253(21)00223-5
13. Zeng Z, Lin H, Jiang M et al (2024) Anti-TNFα in inflammatory bowel disease: from originators to biosimilars. Front Pharmacol 15:1424606. https://doi.org/10.3389/fphar.2024.1424606
14. Hyams JS, Davis Thomas S, Gotman N et al (2019) Clinical and biological predictors of response to standardised paediatric colitis therapy (PROTECT): a multicentre inception cohort study. Lancet 393:1708–1720. https://doi.org/10.1016/S0140-6736(18)32592-3
15. Bokemeyer B, Plachta-Danielzik S, di Giuseppe R et al (2024) Real-world effectiveness of vedolizumab vs anti-TNF in biologic-naive Crohn's disease patients: a 2-year propensity-score-adjusted analysis from the VEDOIBD-study. Inflamm Bowel Dis 30:746–756. https://doi.org/10.1093/ibd/izad138
16. Gubatan J, Holman DR, Puntasecca CJ et al (2021) Antimicrobial peptides and the gut microbiome in inflammatory bowel disease. World J Gastroenterol 27:7402–7422. https://doi.org/10.3748/wjg.v27.i43.7402
17. Hancock REW, Haney EF, Gill EE (2016) The immunology of host defence peptides: beyond antimicrobial activity. Nat Rev Immunol 16:321–334. https://doi.org/10.1038/nri.2016.29
18. Sun J, Chen M, Hu Z et al (2024) Ribonuclease 4 functions as an intestinal antimicrobial protein to maintain gut microbiota and metabolite homeostasis. Nat Commun 15:5778. https://doi.org/10.1038/s41467-024-50223-1
19. Mookherjee N, Anderson MA, Haagsman HP, Davidson DJ (2020) Antimicrobial host defence peptides: functions and clinical potential. Nat Rev Drug Discov 19:311–332. https://doi.org/10.1038/s41573-019-0058-8
20. van der Plas MJA, Bhongir RKV, Kjellström S et al (2016) Pseudomonas aeruginosa elastase cleaves a C-terminal peptide from human thrombin that inhibits host inflammatory responses. Nat Commun 7:11567. https://doi.org/10.1038/ncomms11567
21. Wehkamp J, Stange EF (2020) An update review on the Paneth cell as key to ileal Crohn's disease. Front Immunol 11:646. https://doi.org/10.3389/fimmu.2020.00646
22. Bevins CL, Salzman NH (2011) Paneth cells, antimicrobial peptides and maintenance of intestinal homeostasis. Nat Rev Microbiol 9:356–368. https://doi.org/10.1038/nrmicro2546
23. Ostaff MJ, Stange EF, Wehkamp J (2013) Antimicrobial peptides and gut microbiota in homeostasis and pathology. EMBO Mol Med 5:1465–1483. https://doi.org/10.1002/emmm.201201773
24. Peng Y, Wu Y, Fu Z et al (2026) Amphibian-derived peptide OA-AL14 alleviates UVB-induced skin photoaging via autophagy activation mediated by the AMPK/mTOR pathway. Integr Zool. https://doi.org/10.1111/1749-4877.70134
25. Deng CJ, Wang Y, Yang XW (2026) Amphibian-derived peptides as novel therapeutics for skin wound healing: mechanisms, applications, and challenges. Zool Res 47:727–747. https://doi.org/10.24272/j.issn.2095-8137.2026.076
26. Liu X, Liu J, Li B et al (2026) First identification of an amphibian-derived peptide with anti-vascular aging activity. Zool Res 47:748–764. https://doi.org/10.24272/j.issn.2095-8137.2025.499
27. Fu Z, Xiao Z, Li Y et al (2026) A frog bioactive peptide suppresses inflammation by modulating autophagy for skin wound regeneration. Commun Biol. https://doi.org/10.1038/s42003-026-10766-z
28. Fu Z, Jiang J, Jia Q et al (2026) The self-assembling amphibian-derived peptide (RADA)4-FZ1 pioneers a novel therapeutic platform for diabetic skin wound management. Chem Eng J 530:173231. https://doi.org/10.1016/j.cej.2026.173231
29. Wang J, Yang Y, Ru Z et al (2026) Food-derived peptide RDP3 mitigates pyroptosis to enhance oral mucosal repair via the IL-2Rβ/PI3K axis. NPJ Regen Med. https://doi.org/10.1038/s41536-026-00487-6
30. Chen F, Wang K (2019) Characterization of the innate immunity in the mud crab *Scylla paramamosain*. Fish Shellfish Immunol 93:436–448. https://doi.org/10.1016/j.fsi.2019.07.076
31. Zhang C, Chen F, Bai Y et al (2024) A novel antimicrobial peptide Spasin141-165 identified from *Scylla paramamosain* exhibiting protection against *Aeromonas hydrophila* infection. Aquaculture 591:741137. https://doi.org/10.1016/j.aquaculture.2024.741137
32. Sperstad SV, Haug T, Blencke HM et al (2011) Antimicrobial peptides from marine invertebrates: challenges and perspectives in marine antimicrobial peptide discovery. Biotechnol Adv 29:519–530. https://doi.org/10.1016/j.biotechadv.2011.05.021
33. Tassanakajon A, Rimphanitchayakit V, Visetnan S et al (2018) Shrimp humoral responses against pathogens: antimicrobial peptides and melanization. Dev Comp Immunol 80:81–93. https://doi.org/10.1016/j.dci.2017.05.009
34. Wang K, Zhang C, Chen F, Hao H (2024) An antimicrobial peptide Scymidgutin from *Scylla paramamosain* and its applications. Chinese Patent Application, Publication No. CN117567581A
35. He Y, Li M, Su J et al (2025) Expanding the antimicrobial spectrum of lugdunin: discovery of multi-cationic derivatives of lugdunin with antimicrobial activity against gram-positive and gram-negative bacteria. Eur J Med Chem 299:118078. https://doi.org/10.1016/j.ejmech.2025.118078
36. Jhundoo HD, Siefen T, Liang A et al (2021) Hyaluronic acid increases anti-inflammatory efficacy of rectal 5-amino salicylic acid administration in a murine colitis model. Biomol Ther 29:536–544. https://doi.org/10.4062/biomolther.2020.227
37. Ma WJ, Wang C, Kothandapani J et al (2025) Bespoke plant glycoconjugates for gut microbiota-mediated drug targeting. Science 388:1410–1416. https://doi.org/10.1126/science.adk7633
38. Cullen TW, Schofield WB, Barry NA et al (2015) Antimicrobial peptide resistance mediates resilience of prominent gut commensals during inflammation. Science 347:170–175. https://doi.org/10.1126/science.1260580
39. Destoumieux-Garzón D, Rosa RD, Schmitt P et al (2016) Antimicrobial peptides in marine invertebrate health and disease. Philos Trans R Soc Lond B Biol Sci 371:20150300. https://doi.org/10.1098/rstb.2015.0300
40. Brogden KA (2005) Antimicrobial peptides: pore formers or metabolic inhibitors in bacteria? Nat Rev Microbiol 3:238–250. https://doi.org/10.1038/nrmicro1098
41. Nijnik A, Hancock REW (2009) The roles of cathelicidin LL-37 in immune defences and novel clinical applications. Curr Opin

Hematol 16:41–47. https://doi.org/10.1097/MOH.0b013e32831ac517
42. Bhattacharjya S, Zhang Z, Ramamoorthy A (2024) LL-37: structures, antimicrobial activity, and influence on amyloid-related diseases. Biomolecules 14:320. https://doi.org/10.3390/biom14030320
43. Yuan Y, Li J, Wei G et al (2025) Exploring the antimicrobial potential of LL-37 derivatives: recent developments and challenges. ACS Biomater Sci Eng 11:3145–3164. https://doi.org/10.1021/acsbiomaterials.4c02029
44. Shapouri-Moghaddam A, Mohammadian S, Vazini H et al (2018) Macrophage plasticity, polarization, and function in health and disease. J Cell Physiol 233:6425–6440. https://doi.org/10.1002/jcp.26429
45. Murray PJ, Allen JE, Biswas SK et al (2014) Macrophage activation and polarization: nomenclature and experimental guidelines. Immunity 41:14–20. https://doi.org/10.1016/j.immuni.2014.06.008
46. Matsuzaki K (2009) Control of cell selectivity of antimicrobial peptides. Biochim Biophys Acta 1788:1687–1692. https://doi.org/10.1016/j.bbamem.2008.09.013
47. Xavier RJ, Podolsky DK (2007) Unravelling the pathogenesis of inflammatory bowel disease. Nature 448:427–434. https://doi.org/10.1038/nature06005
48. Glocker EO, Kotlarz D, Klein C et al (2011) IL-10 and IL-10 receptor defects in humans. Ann N Y Acad Sci 1246:102–107. https://doi.org/10.1111/j.1749-6632.2011.06339.x
49. Lloyd-Price J, Arze C, Ananthakrishnan AN et al (2019) Multi-omics of the gut microbial ecosystem in inflammatory bowel diseases. Nature 569:655–662. https://doi.org/10.1038/s41586-019-1237-9
50. Nicholson JK, Holmes E, Kinross J et al (2012) Host-gut microbiota metabolic interactions. Science 336:1262–1267. https://doi.org/10.1126/science.1223813
51. Stange EF (2024) Dysbiosis in inflammatory bowel diseases: egg, not chicken. Front Med 11:1395861. https://doi.org/10.3389/fmed.2024.1395861
52. Shukla PK, Meena AS, Rao V et al (2018) Human defensin-5 blocks ethanol and colitis-induced dysbiosis, tight junction disruption and inflammation in mouse intestine. Sci Rep 8:16241. https://doi.org/10.1038/s41598-018-34263-4
53. Zheng D, Liwinski T, Elinav E (2020) Interaction between microbiota and immunity in health and disease. Cell Res 30:492–506. https://doi.org/10.1038/s41422-020-0332-7
54. Han F, Zhang H, Xia X et al (2015) Porcine β-defensin 2 attenuates inflammation and mucosal lesions in dextran sodium sulfate-induced colitis. J Immunol 194:1882–1893. https://doi.org/10.4049/jimmunol.1402300
55. Rosa LF, Rings A, Stolzer I et al (2023) Human α-defensin $5_{1-9}$ and human β-defensin 2 improve metabolic parameters and gut barrier function in mice fed a Western-style diet. Int J Mol Sci 24:13878. https://doi.org/10.3390/ijms241813878
56. Zhang Y, Guo C, Li Y et al (2022) Alginate oligosaccharides ameliorate DSS-induced colitis through modulation of AMPK/NF-κB pathway and intestinal microbiota. Nutrients 14:2864. https://doi.org/10.3390/nu14142864
57. Frank DN, St Amand AL, Feldman RA et al (2007) Molecular-phylogenetic characterization of microbial community imbalances in human inflammatory bowel diseases. Proc Natl Acad Sci U S A 104:13780–13785. https://doi.org/10.1073/pnas.0706625104
58. Earle KA, Billings G, Sigal M et al (2015) Quantitative imaging of gut microbiota spatial organization. Cell Host Microbe 18:478–488. https://doi.org/10.1016/j.chom.2015.09.002
59. Lopez-Siles M, Enrich-Capó N, Aldeguer X et al (2018) Alterations in the abundance and co-occurrence of *Akkermansia muciniphila* and *Faecalibacterium prausnitzii* in the colonic mucosa of inflammatory bowel disease subjects. Front Cell Infect Microbiol 8:281. https://doi.org/10.3389/fcimb.2018.00281
60. Zeng MY, Inohara N, Nuñez G (2017) Mechanisms of inflammation-driven bacterial dysbiosis in the gut. Mucosal Immunol 10:18–26. https://doi.org/10.1038/mi.2016.75
61. Chassaing B, Aitken JD, Malleshappa M, Vijay-Kumar M (2014) Dextran sulfate sodium (DSS)-induced colitis in mice. Curr Protoc Immunol 104:15.25.1-15.25.14. https://doi.org/10.1002/0471142735.im1525s104
62. Wirtz S, Neufert C, Weigmann B, Neurath MF (2007) Chemically induced mouse models of intestinal inflammation. Nat Protoc 2:541–546. https://doi.org/10.1038/nprot.2007.41
63. Neurath MF (2014) Cytokines in inflammatory bowel disease. Nat Rev Immunol 14:329–342. https://doi.org/10.1038/nri3661
64. Fiebiger U, Bereswill S, Heimesaat MM (2016) Dissecting the interplay between intestinal microbiota and host immunity in health and disease: lessons learned from germfree and gnotobiotic animal models. Eur J Microbiol Immunol 6:253–271. https://doi.org/10.1556/1886.2016.00036
65. Kennedy EA, King KY, Baldridge MT (2018) Mouse microbiota models: comparing germ-free mice and antibiotics treatment as tools for modifying gut bacteria. Front Physiol 9:1534. https://doi.org/10.3389/fphys.2018.01534
66. Swidsinski A, Ladhoff A, Pernthaler A et al (2002) Mucosal flora in inflammatory bowel disease. Gastroenterology 122:44–54. https://doi.org/10.1053/gast.2002.30294
67. Swidsinski A, Loening-Baucke V, Herber A (2009) Mucosal flora in Crohn's disease and ulcerative colitis—an overview. J Physiol Pharmacol 60(Suppl 6):61–71
68. Lu Y, Zhang B, Wang Z et al (2026) From host-derived pressures to the environmental anti-antimicrobial peptides resistome: mechanisms, reservoirs and implications for therapeutic peptide design. Mar Drugs 24:76. https://doi.org/10.3390/md24020076
69. Brinch KS, Frimodt-Møller N, Høiby N, Kristensen HH (2009) Influence of antidrug antibodies on plectasin efficacy and pharmacokinetics. Antimicrob Agents Chemother 53:4794–4800. https://doi.org/10.1128/AAC.00440-09
70. Hemmer B, Kondo T, Gran B et al (2000) Minimal peptide length requirements for $CD4^+$ T cell clones—implications for molecular mimicry and T cell survival. Int Immunol 12:375–383. https://doi.org/10.1093/intimm/12.3.375
71. Chen CH, Chiu YC, Huang KY et al (2025) A reproducible sequence-level strategy to enhance peptide immunogenicity while preserving wild-type epitope recognition. Antibodies 14:106. https://doi.org/10.3390/antib14040106
72. Dam T, Sharma P, Kaur P et al (2026) Engineering peptide-based hydrogels: smart therapeutic platforms for inflammatory disorders. ACS Biomater Sci Eng 12:1868–1912. https://doi.org/10.1021/acsbiomaterials.5c01852
73. Colomina-Alfaro L, Marchesan S, Stamboulis A, Bandiera A (2023) Smart tools for antimicrobial peptides expression and application: the elastic perspective. Biotechnol Bioeng 120:323–332. https://doi.org/10.1002/bit.28283

**Publisher's Note** Springer Nature remains neutral with regard to jurisdictional claims in published maps and institutional affiliations.

Springer Nature or its licensor (e.g. a society or other partner) holds exclusive rights to this article under a publishing agreement with the author(s) or other rightsholder(s); author self-archiving of the accepted manuscript version of this article is solely governed by the terms of such publishing agreement and applicable law.